UCRL-ID-104576
PATC-IR 89-11

STRUCTURAL IMPACT ANALYSES

April 10, 1990

M. C. Witte

Prepared for
U.S. Nuclear Regulatory Commission

DISCLAIMER

This work was supported by the United States Nuclear Regulatory Commission under a Memorandum of Understanding with the United States Department of Energy.

PATC-IR 89-11

STRUCTURAL IMPACT ANALYSES

April 10, 1990

M. C. Witte

Prepared for
U.S. Nuclear Regulatory Commission

ABSTRACT

Section 5062 of Public Law 100-203 is concerned with air shipment of plutonium from one foreign country to another through United States airspace. It applies specifically to the packages in which the plutonium is shipped, requiring that the packages be certified by the NRC as safe for the purpose and that the packages must be able to survive the worst aircraft accident without releasing significant quantities of the plutonium contents.

The law requires actual tests to be conducted in the certification process. Actual tests include drop tests of the package or a crash test of the cargo aircraft with test packages aboard to replicate actual worst-case aircraft accident conditions unless the stresses produced by design tests exceed the stresses produced by actual crash tests. The NRC specified that the conditions associated with the crash of PSA Flight 1771 on December 7, 1987, represents a worst-case aircraft accident and therefore are suitable for use as the basis for conducting the required tests.

In order to assure adequacy of testing, both of the individual packages and of the cargo aircraft, a series of analyses have been performed. This report documents the analyses performed for a basis package and for simplified models of two aircraft fuselages.

TABLE OF CONTENTS

ACKNOWLEDGEMENTS

The work described in this report was carried out in support of the Plutonium Air Transport Certification (PATC) Program, conducted by the Nuclear Systems Safety Program (NSSP) at Lawrence Livermore National Laboratory for the U.S. Nuclear Regulatory Commission (NRC). John Jankovich and John Cook of the NRC provided guidance of this work.

Carl Walter and Larry Fischer provided valuable technical and administrative reviews of this report. C.K. Chou provided expert program leadership for administrative guidance and support. Jerry Goudreau gave valuable assistance in the target model development.

Finally, Lisa Hensel, Ellen Sturmer, and Merry Carter provided typing and publication services.

1. INTRODUCTION

1.1 Background

Section 5062 of Public Law 100-203 is concerned with air shipment of plutonium from one foreign country to another through United States airspace. It applies specifically to the packages in which the plutonium is shipped, requiring that the packages be certified by the NRC as safe for the purpose and that the packages must be able to survive the worst aircraft accident without releasing significant quantities of the plutonium contents.

The law requires actual tests to be conducted in the certification process. Actual tests include drop tests of the package or a crash test of the cargo aircraft with test packages aboard to replicate actual worst-case aircraft accident conditions unless the stresses produced by design tests exceed the stresses produced by actual crash tests. The NRC specified that the conditions associated with the crash of PSA Flight 1771 on December 7, 1987, represents a worst-case aircraft accident and therefore are suitable for use as the basis for conducting the required tests.

In order to assure adequacy of testing, both of the individual packages and of the cargo aircraft, a series of analyses have been performed. This report documents the analyses performed for a basis package and for simplified models of two aircraft fuselages.

1.2 Basis PAT Package Used for Analyses

The PAT-1 package (Ref. 1) has been certified to be safe by the NRC, and it is exempted from meeting the requirements of Section 5062 of Public Law 100-203. Also, the PAT-1 package is in Fissile Class I, which means that: (1) it may be transported in unlimited numbers; and (2) assignment of a transport index to assure nuclear criticality safety is not required. The approximate external dimensions of the PAT-1 package are: diameter 0.6 m and height 1.1 m. The PAT-1 package weighs 225 kg and has a maximum capacity of 2 kg of PuO_2.

It is reasonable to assume that if the PAT-1 package is not used, larger packages will be desired. We selected as the basis PAT package a design that, in comparison to the PAT-1 package, has its dimensions increased by a factor of 2 (approximately).

Although one might expect the resulting package to weigh eight times as much, we modified this outcome for the basis package. We assume that the total package mass is further increased by a factor of 1.6 to account for the heavier structure that may be needed to withstand the higher impact speed of the aircraft-crash test. We also assume that the plutonium capacity is reduced by a factor of two (i.e., increased by a factor of four, not eight over the PAT-1 capacity) to meet the criticality criterion. Thus, our basis PAT package is cylindrical with these dimensions and capacities: diameter 1.2 m, height 2.6 m, total mass 2.9 Mg, and plutonium oxide powder

capacity 8 kg. The basis PAT package consists of an outer containment vessel, an inner limiter, a load spreader, an outer limiter, and an outer steel shell as shown in Fig. 1-1.

The package used in all analyses is the basis package described above. Assumptions have been made about materials and dimensions, as required to perform analyses. Several different finite element models of the package were used, depending upon the type of analysis. The finite element models are described with each analysis.

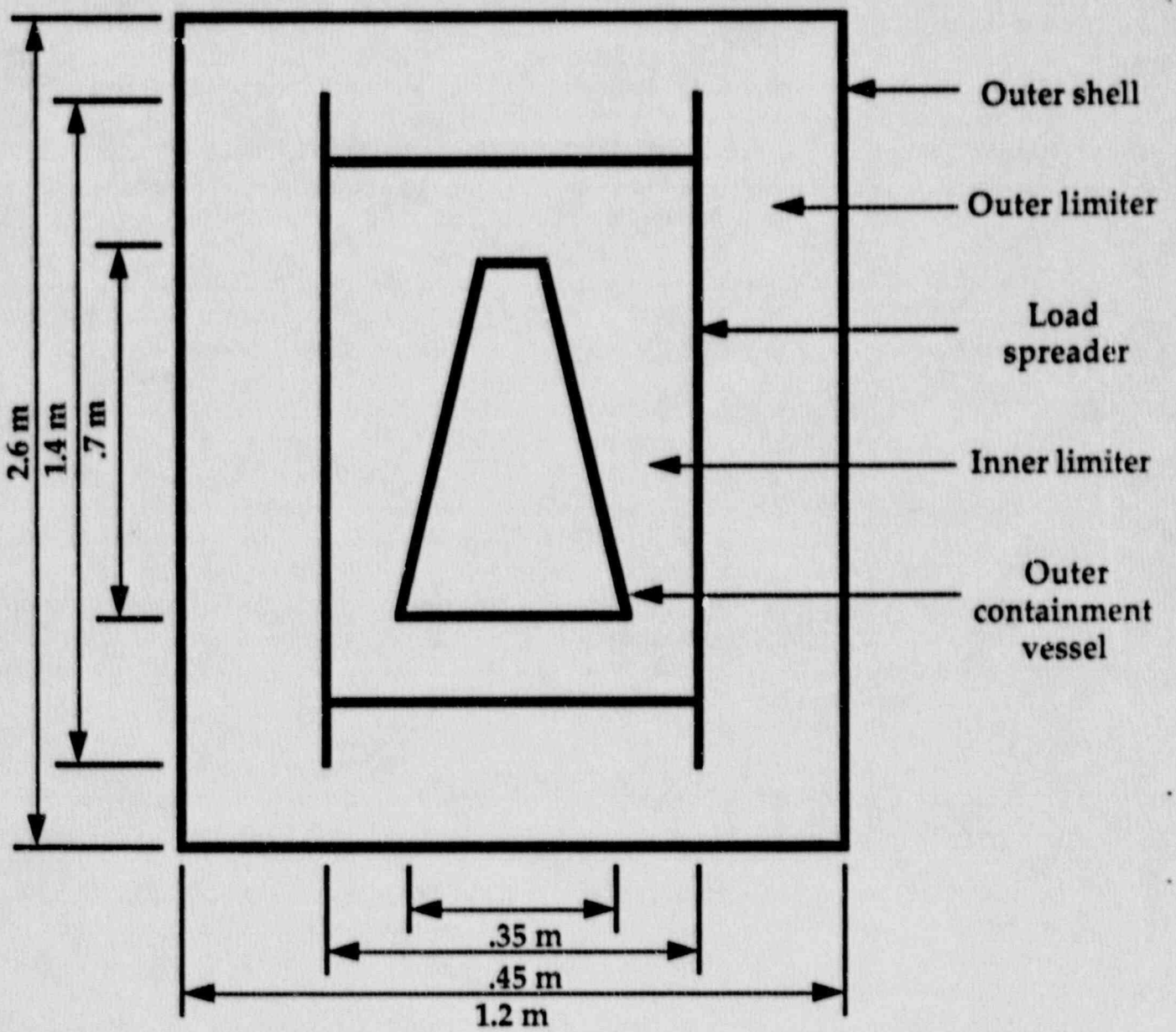

Fig. 1-1. Basis package model.

2. PA KAGE MATERIALS

2.1 Effects Due to High Strain Rates

Because an aircraft crash environment will result in a high loading rate both on the aircraft and its components, and on the package, it is necessary to consider the effects of high strain rates on the behavior of the material in the aircraft and in the package. Two categories of materials are discussed: metals and wood.

2.1.1 Metals

Metals are inherently rate dependent, though variation of the yield stress with strain rate can be low (Ref. 2). It appears that ductile metals show more pronounced strain rate hardening than less ductile metals (Ref. 3). Frequently associated with high strain rates are large strains and high temperatures. It is difficult to separate the effects of strain rate hardening and thermal softening at large strains and high strain rates. At large strains significant heat is generated due to plastic work, and at high strain rates there is not time for the heat to be conducted away so that adiabatic heating of the material results (Ref. 4). The effect of this is to decrease the work hardening rate due to thermal softening (see Refs. 2 and 4). Some stress strain curves (for torsional loading) for various strain-rates are shown in Figs. 2-1 and 2-2 (from G. R. Johnson, et al., Refs. 3 and 4). Figures 2-3, 2-4, and 2-5 show the effect of strain rate on strain at failure for some metals (Refs. 3 and 4).

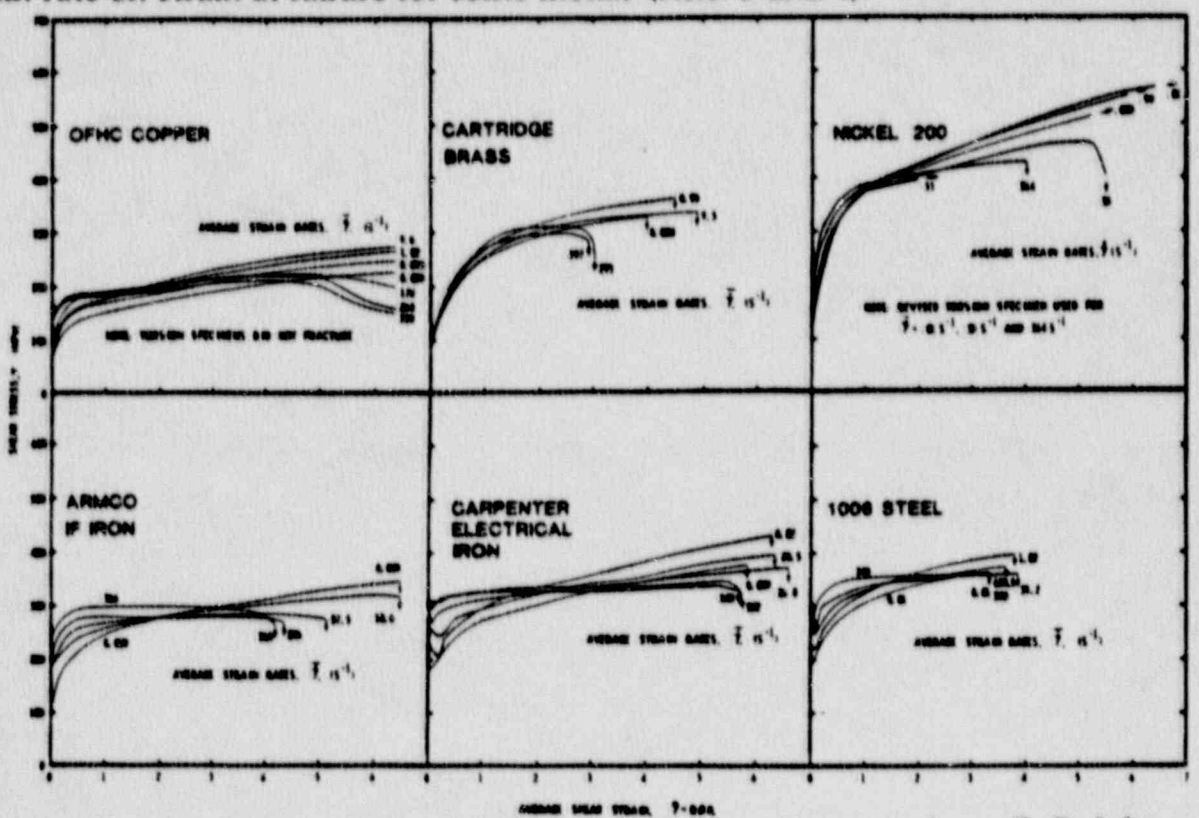

Fig. 2-1. Torsional stress-strain test data at various strain rates, from G. R. Johnson, et al, Ref. 3.

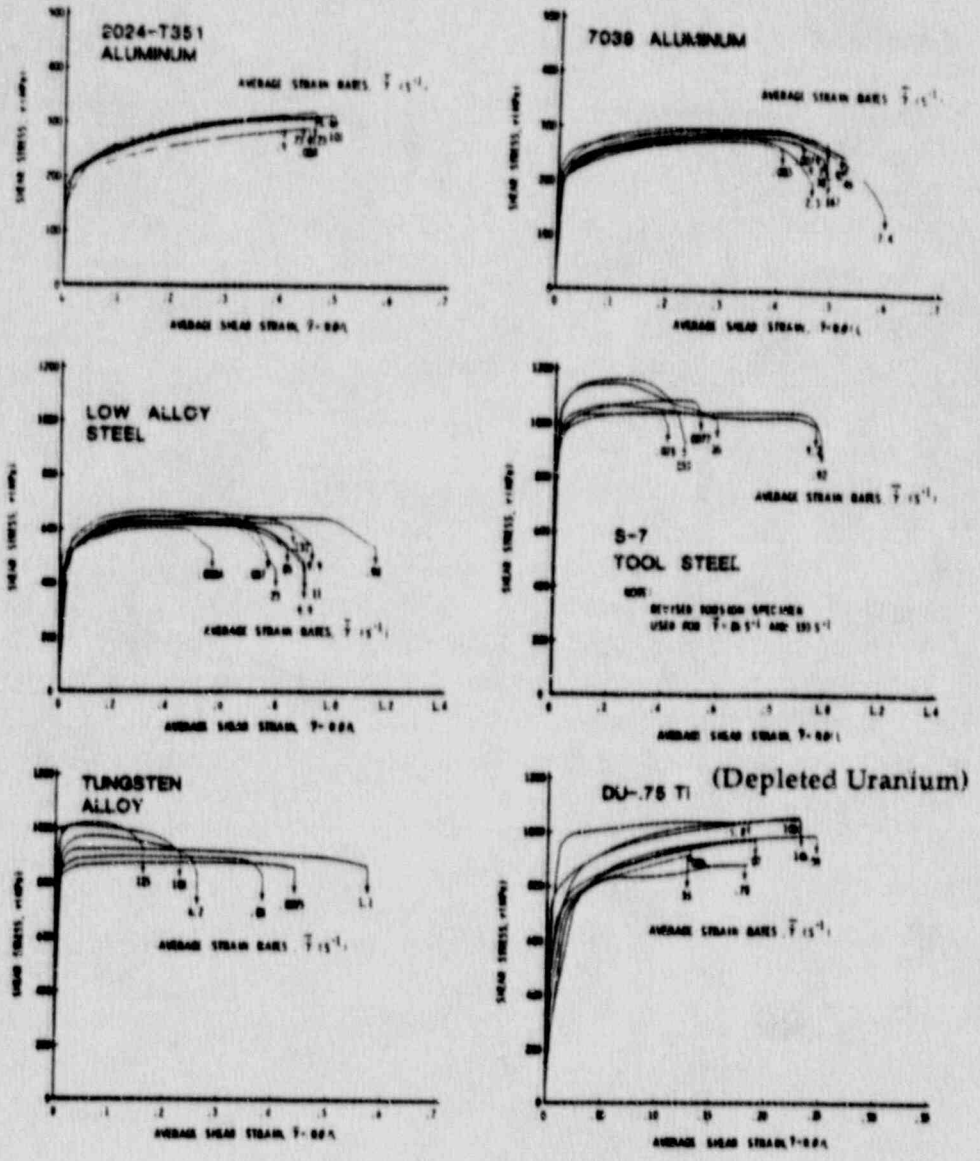

Fig. 2-2. Torsional stress-strain test data at various strain rates, from G. R. Johnson, et al., Ref. 4.

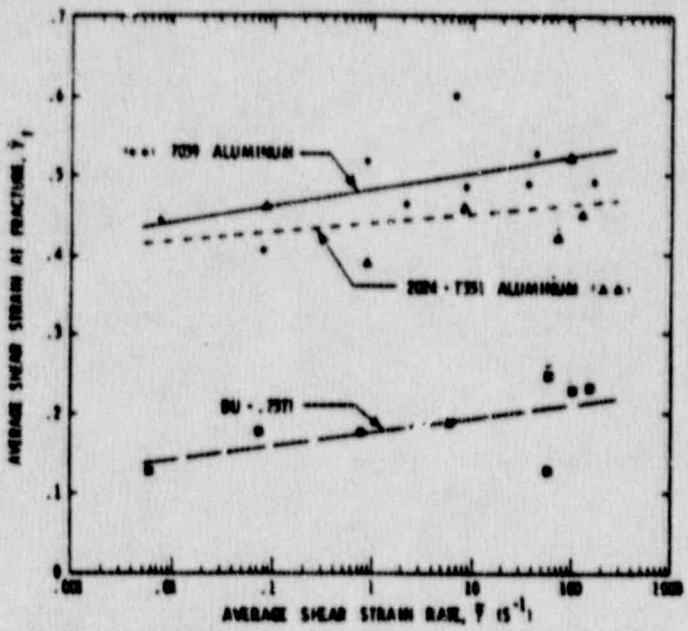

Fig. 2-3. Effect of strain rate on the average shear strain at fracture for 2024-T351 aluminum, 7039 aluminum DU-.75Ti, from G. R. Johnson, et al., Ref. 4.

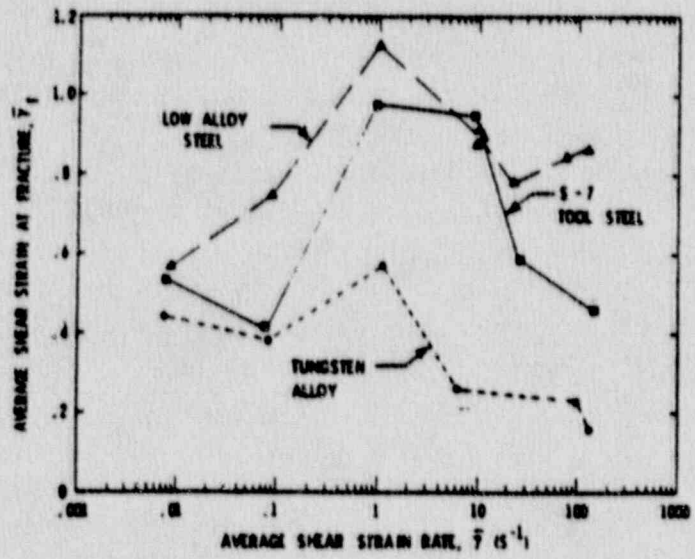

Fig. 2-4. Effect of strain rate on the average shear strain at fracture for low allow steel, S-7 tool steel and tungsten alloy, from G. R. Johnson, et al., Ref. 4.

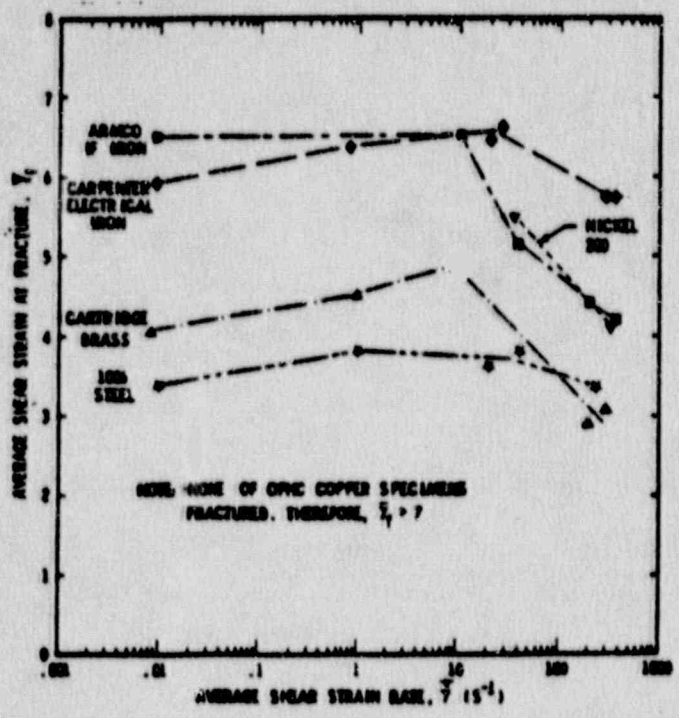

Fig. 2-5. Effect of strain rate on the average shear strain at fracture, from G. R. Johnson, et al., Ref. 3.

In order to apply this information to the aircraft and the package, we must look at available data on 2024-T4 aluminum (aircraft) and on stainless steels and various other metal alloys (package), for the range of strain rates expected. This range is from 10 s^{-1} to 10^2 s^{-1} for the package containment vessel based on finite element analyses, and is most likely much higher for the aircraft. Data shown in Figs. 2-2 and 2-3 from Ref. 3 indicate that 2024-T351 aluminum is not highly strain sensitive. Other researchers (Ref. 5) reach similar conclusions. No strain rate data are available on 2024-T4 aluminum, however the heat treatments T4 and T351 are very similar. Figure 2-6 (from Ref. 2) shows stress-strain curves as a function of strain rate for 304L stainless steel. One can see that the yield stress in 304L is strongly strain-rate dependent. However, for the strain rate range 2×10^{-4} s^{-1} to 10^2 s^{-1} the strain to failure does not vary substantially. Stout notes that in many FCC metals, the rate sensitivity increases at high strain rates; in 304L the increase begins when the strain rate exceeds 10^2 s^{-1} (Ref. 2). Strain rate effects on titanium alloys have not been published and are not included in this report. Data on pure alpha titanium (Ref. 6) suggest that like other metals, the yield stress increases markedly with increasing strain rates.

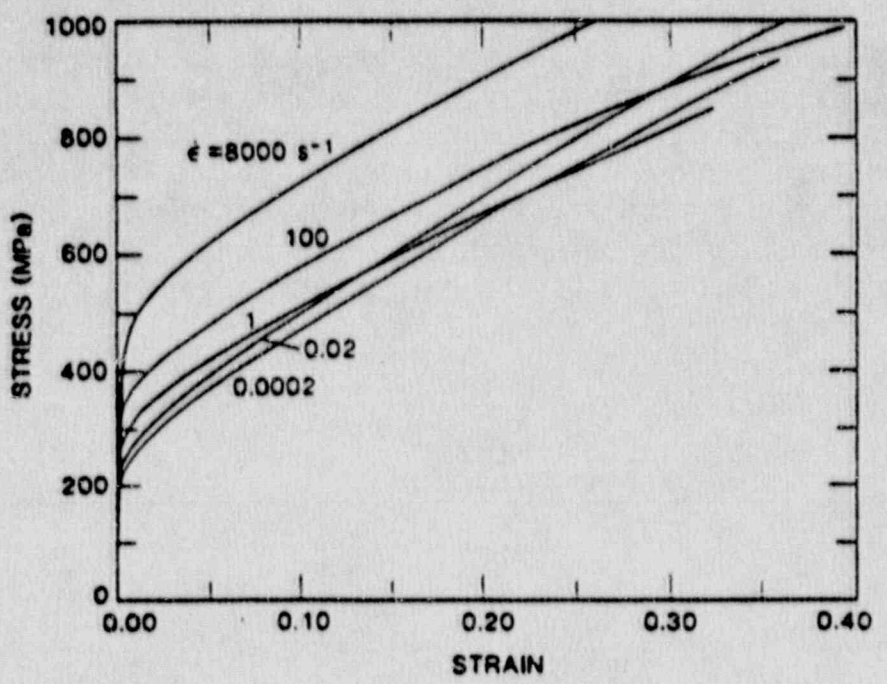

Fig. 2-6. Stress/strain curves for the 304L rod stock compressed at strain rates between 2 x 10^{-4} s^{-1} and 1 x 10^{4} s^{-1}, from M. G. Stout and P. S. Follansbee, Ref. 2.

2.1.2 Wood

The behavior of wood as a function of rate of loading has been studied by a number of researchers (see Ref. 7 through 11), although very little experimental work has been published at strain rates above 0.1 s^{-1}. Available data indicate that for soft woods there is no significant effect of load rate on the modulus of elasticity; the yield stress increases with increase in load rate; and the ultimate strength increases with increase in load rate (Ref. 8). The maximum crush strength parallel to the grain increases from 4700 psi to 6200, with an increase in strain rate from $3.6x10^{-4}$ s^{-1} to $1.2x10^{-4}$ s^{-1}, for Sitka spruce (Ref. 7). Since a strain rate in the range of at least 10^{3} s^{-1} is expected for a redwood limiter during the high velocity (930 ft/s) impact event (based on finite element analyses), the data can only be used to suggest that the crush strength will be higher than published values based on static tests.

2.2 Limiter

Redwood is a good selection for an impact limiter for two reasons: it has a high specific energy absorption capability parallel to the grain, outranking most other shock mitigators such as foams and honeycombs; and because redwood compares favorably with other impact energy absorbers in char performance (Ref. 12). The behavior of the limiter governs the overall behavior of the package during impact. The wood was modeled for finite element analyses of the package using DYNA's

material Type 5 (soil and crushable foam). The inputs required for this model are a pressure vs volumetric strain curve, a yield function, and elastic properties. The wood is assumed to fail in tension at 200 psi. Wood density was determined based on the calculated volume of the limiter in the basis package and a mass allowance for the stainless steel overpack in the limiter density. The published crush strength of redwood varies from about 5000 psi to about 7000 psi, depending on temperature and reference (Refs. 12 and 13). Redwood properties vary considerably depending upon direction of loading. Wood is substantially stronger parallel to the grain, both in tension and compression, than it is perpendicular to the grain. Wood properties as modeled are listed in Table 2-1.

Table 2-1. Redwood properties used in model.

	Perpendicular to Impact	**Parallel to Impact**
Density, lb s^2/in^4	9.5675×10^{-5}	9.5675×10^{-5}
Shear modulus, psi	5.583×10^5	5.583×10^5
Bulk unloading modulus, psi	5.5×10^7	5.5×10^7
Yield curve constants:		
a^0	1.633×10^5	1.2×10^7
a^1	0	0
a^2	0	0
Pressure cutoff, psi	-200	-200
Pressure/volumetric strain relationships		
Vol. strain: $\ln\left(\frac{V_{new}}{V_o}\right)$	Pressure (psi)	
0.	0	0
-4.5×10^{-3}	7.0×10^2	6.0×10^3
-1.2	7.0×10^2	6.0×10^3
-4.6	5.2×10^7	5.2×10^7

2.3 Containment Vessel Alloy

The outer containment vessel is made from a metal alloy. The alloy is assumed to behave in an elastic-perfectly plastic manner, with a yield stress of 110 ksi. Properties used in the model are tabulated in Table 2-2.

Table 2-2. Containment vessel alloy properties used in the model.

Density, lb s^2/in^4	6.4120×10^{-4}
Young's modulus, psi	1.7×10^7
Poisson's ratio	0.33
Yield stress, psi	1.1×10^5
Hardening modulus, psi	0

2.4 Inner Limiter

The annulus between the load spreader and the outer containment vessel is made from redwood and contains other materials to enhance heat transfer and improve structural capability. This material is modeled with the same material properties as redwood. The actual material will be somewhat stiffer due to the presence of heat transfer and structural components. This should not have a significant effect on the results, since the assumed volume of the inner limiter is small relative to the overall volume of the package.

2.5 Load Spreader

The load spreader of the package is made from a high strength stainless steel. This is a stainless steel with roughly twice the yield strength of Type 316 steel, with better corrosion resistance. Properties in bar form are listed in Table 2-3. The load spreader is modeled as an elastic-perfectly plastic material with a yield stress of 60,000 psi.

Table 2-3. Load spreader alloy properties used in the model.

Density, lb s^2/in^4	6.614×10^{-4}
Young's modulus, psi	2.8×10^7
Poisson's ratio	0.29
Yield stress, psi	6.0×10^4
Hardening modulus, psi	0

3. ANALYSES OF THE BASIS PAT PACKAGE FOR IMPACT ON AN UNYIELDING SURFACE IN TWO ORIENTATIONS

3.1 Geometry and Mesh

Analyses were performed for side and end impact orientations of the basis package. All analyses were completed using DYNA 2D and DYNA 3D. The analyses were performed on the package geometry shown in Section 1. The model includes the stainless steel load spreader, and a metal alloy inner container. It does not include any details of the containment vessel closure system, nor does it include any detail inside of this containment vessel (e.g. inner containment vessel or powder cans). The outer steel shell has not been explicitly modeled, however, the effect of this shell has been taken into account by means of the boundary conditions on the wood limiter. These are as follows: the boundary nodes on the wood are constrained to move only in the direction of the initial velocity. Thus no slumping behavior of the wood is permitted. The contents of the outer containment vessel are not modeled explicitly. Its contents are assigned a reasonable mass and are assumed to have the strength of redwood. The initial analyses were run with the limiter modeled as a homogeneous material, with properties of wood crushing in the direction parallel to the wood grain. Subsequent analyses were run with wood properties explicitly input as parallel or perpendicular to the crush direction.

3.2 Material Properties

Material properties are as described in Section 2 of this report, with the exception of the inner and outer wood limiter. Because the behavior of the limiter is so important in the overall behavior of the package during impact, a preliminary study was performed to evaluate the effects of several different sets of redwood input parameters, all used in the homogeneous model with DYNA material Type 5. The different redwoods tested have different crush strengths and initial yield conditions — otherwise they are alike. Different wood properties were selected to provide a range of inputs for these parameters. Wood properties used in this study are listed in Table 3-1. The final analyses, using a model with wood input explicitly as parallel or perpendicular to the direction of impact, use wood properties as provided in Section 2. The wood denoted as Wood 4 was selected for use as the parallel to impact wood for the final analyses.

Table 3-1. Redwood properties used with DYNA material Type 5.

	Wood 1	Wood 2	Wood 3	Wood 4
Density, lb s^2/in^4	9.5675×10^{-5}	9.5675×10^{-5}	9.5675×10^{-5}	9.5675×10^{-5}
G, psi	5.583×10^5	5.583×10^5	5.583×10^5	5.583×10^5
K_u, psi	5.5×10^7	5.5×10^7	5.5×10^7	5.5×10^7
Yield curve constants:				
a^0	1.633×10^5	1.633×10^5	1.633×10^5	1.2×10^7
a^1	0	0	0	0
a^2	0	0	0	0

Volumetric strain/pressure relationships

Vol. strain: $\ln\left(\frac{V_{new}}{V_o}\right)$	Pressure (psi)			
0	0	0	0	0
-.0045	6000.	12000.	18000.	6000.
-1.2	6000.	12000.	18000.	6000.
-4.6	5.2×10^7	5.2×10^7	5.2×10^7	5.2×10^7

3.3 Analyses

3.3.1 End-Impact Preliminary Analyses

The end-impact is analyzed with DYNA 2D (Ref. 14). A horizontal stonewall is the finite element tool which represents the unyielding surface. It is perfectly unyielding. All end impacts were run with the wide side of the containment vessel on the impact end. Three preliminary end impact analyses are run with an initial velocity of 422 ft/s, using redwood materials Wood 1, Wood 3, and Wood 4, as listed in Table 3-1. Results for these runs are listed in Table 3-2. The final end impact analyses were performed at a range of velocities (see Section 3.5).

Table 3-2. Preliminary end impact results using 3D mesh, initial velocity = 422 ft/s.

Redwood Model	Δv/Δt (g)	Max. effective stress in outer containment vessel (psi)	Max. effective plastic strain in inner container %
Wood 1	2980	24,000	0
Wood 2	N/A	N/A	N/A
Wood 3	3700	110,000	0.7
Wood 4	3450	39,800	0

Table 3-3. Preliminary side impact results using 3D mesh, Initial velocity = 422 ft/s.

Redwood Model	Δv/Δt (g)	Max. effective stress in outer containment vessel (psi)	Max. effective plastic strain in inner container %
Wood 1	5700	110,000	.3
Wood 2	8550	110,000	.75
Wood 3	9200	110,000	.75
Wood 4	7100	110,000	0

3.3.2 Side-Drop

The side impact was analyzed with both DYNA 2D and DYNA 3D. Finite element models are shown in Figs. 3-1 and 3-2. Four preliminary side impact analyses were run with an initial velocity of 422 ft/s, using redwood materials Wood 1, Wood 2, Wood 3 and Wood 4. Results for these preliminary runs are listed in Table 3-3. The 2D model was used for the final analyses at a range of velocities, so that the results could be compared to the side impact onto various soils, which were also run with DYNA 2D, in order to save on computer cost. The 2D model eliminates the stiffening effect of the package ends, and is therefore more flexible than the actual package. A comparison of decelerations and effective plastic strains for both models impacting at 422 ft/s is provided in Table 3-4.

Table 3-4. Comparison of 2D and 3D results for side drop at 422 ft/s.

Geometry	Δv/Δt (g)	Max. effective plastic strain in containment (%)
2D	6354	10.4
3D	7100	0.

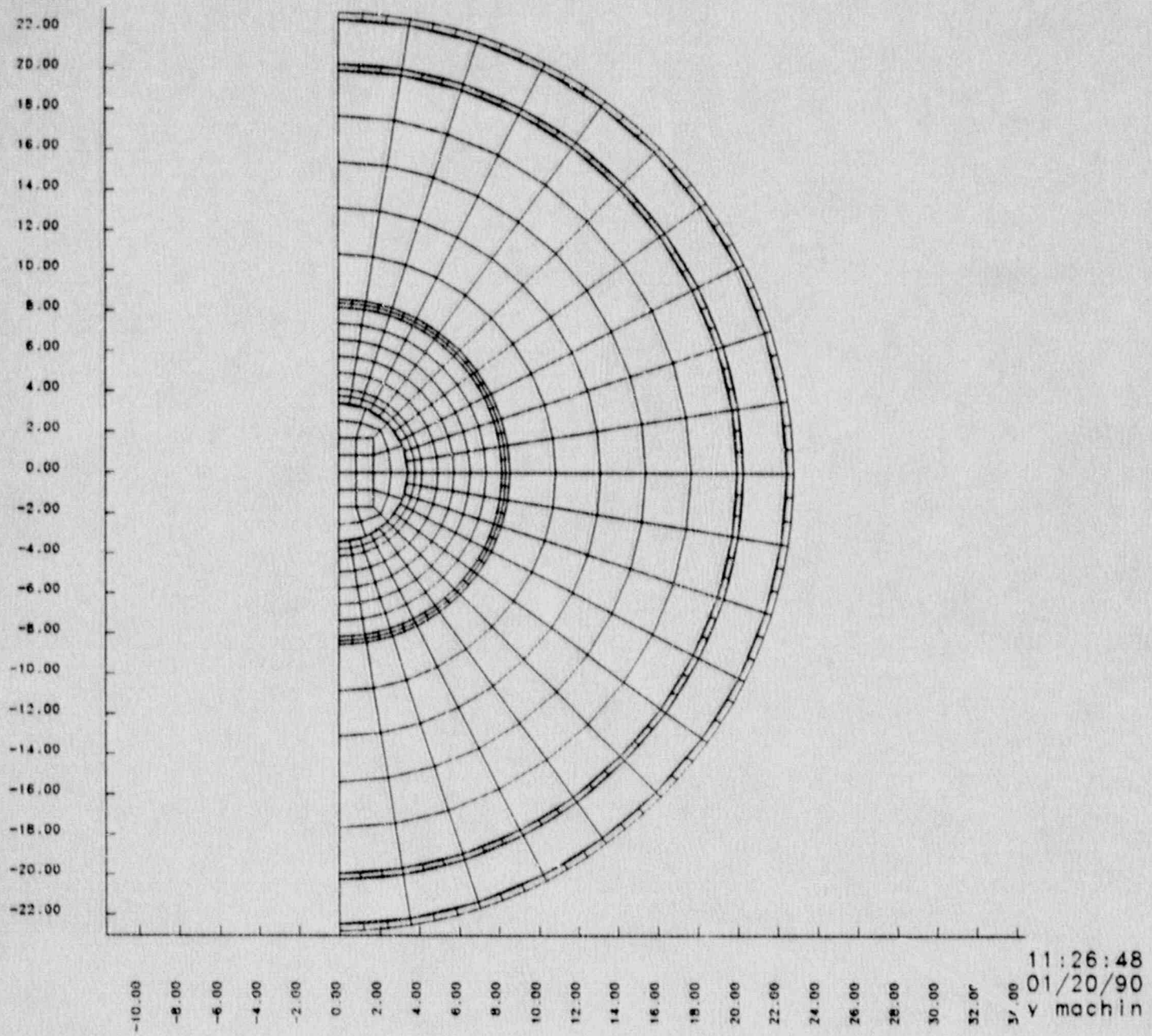

Fig. 3-1. Finite element mesh for 2D side impact analyses.

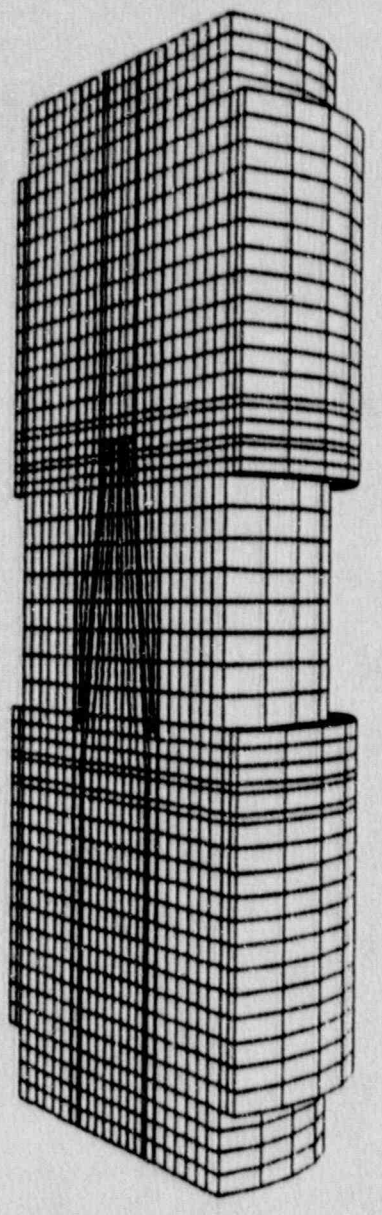

Fig. 3-2. Finite element mesh for 3D side impact analyses.

3.4 Assumptions

Two important assumptions have been made in these analyses. The first is that the closure system of the metal alloy containment vessel is no weaker than the rest of the vessel since the closure was not explicitly modeled. The second assumption is that the redwood limiter must act as a unit. The steel outer cover on the redwood must contain the redwood, and must prevent it from breaking and flying apart away from the package. The analyses summarized in this report do not predict whether or not the steel cover will perform this service, and further analyses are necessary in order to evaluate further this question.

3.5 Results and Conclusions

Final results for the side and end impacts onto an unyielding surface are given in Tables 3-5 and 3-6. In these tables, peak load refers to the peak accelerations read from an acceleration-time history of the analyses. In the next column, average load refers to a value of $\Delta v/\Delta t$ calculated from the steepest portion of the velocity-time history. For the higher velocity impacts, it was not possible to run these problems to completion (i.e. to zero velocity) because of the significant distortion in the mesh. As a result it is not possible to obtain resulting effective plastic strain in every case. These results can be used to compare the severity of different impact orientations. They can not be used to predict package failure based on plastic strain.

Table 3-5. Results of 2D end impact onto an unyielding surface for a range of velocities.

	G Loads on Containment	
Velocity (ft/s)	Peak load (g)	Average load (g)
422	4032	3343
500	4958	3724
525	5269	4119
550	5659	4155
600	6547	4638
650	7062	5258
700	9535	6680
750	12509	11740

Table 3-6. Results of 2D side impact onto an unyielding surface for a range of velocities

	G Loads on Containment	
Velocity (ft/s)	Peak load (g)	Average load (g)
422	7446	6354
500	7897	6517
600	7335	7261
700	8731	8652
800	11726	11067
930	21801	18902

4. ANALYSES OF THE BASIS PACKAGE FOR IMPACT ONTO SEVERAL SOILS IN TWO ORIENTATIONS

4.1 Geometry and Mesh

Impact analyses were performed for side and end impact orientations onto three ground surfaces (granite, weathered rock, and medium stiffness soil) for the basis PAT package. All analyses were performed on the package geometry used in the final analyses described in Section 3. The finite element meshes used are shown in Figs. 4-1 and 4-2. The targets are modeled as semi-infinite half spaces, with the target boundary being far enough away from the location of impact so that the time for the shear wave to make a round trip from impact to boundary is longer than the duration of the impact itself. A 2D mesh was used for the side impact condition as discussed in Section 3.2.

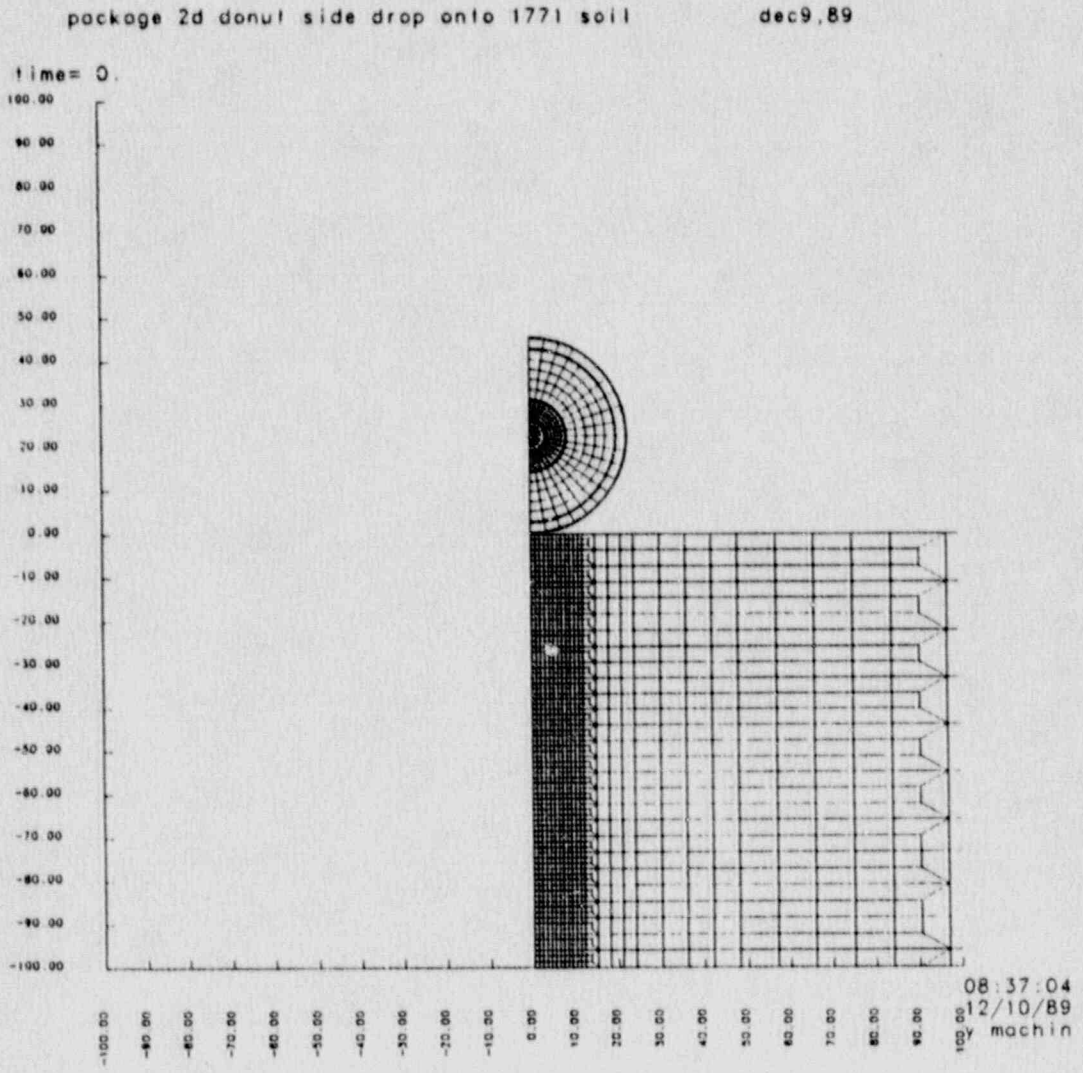

Fig. 4-1. Two-dimensional finite element mesh for side impact onto various surfaces.

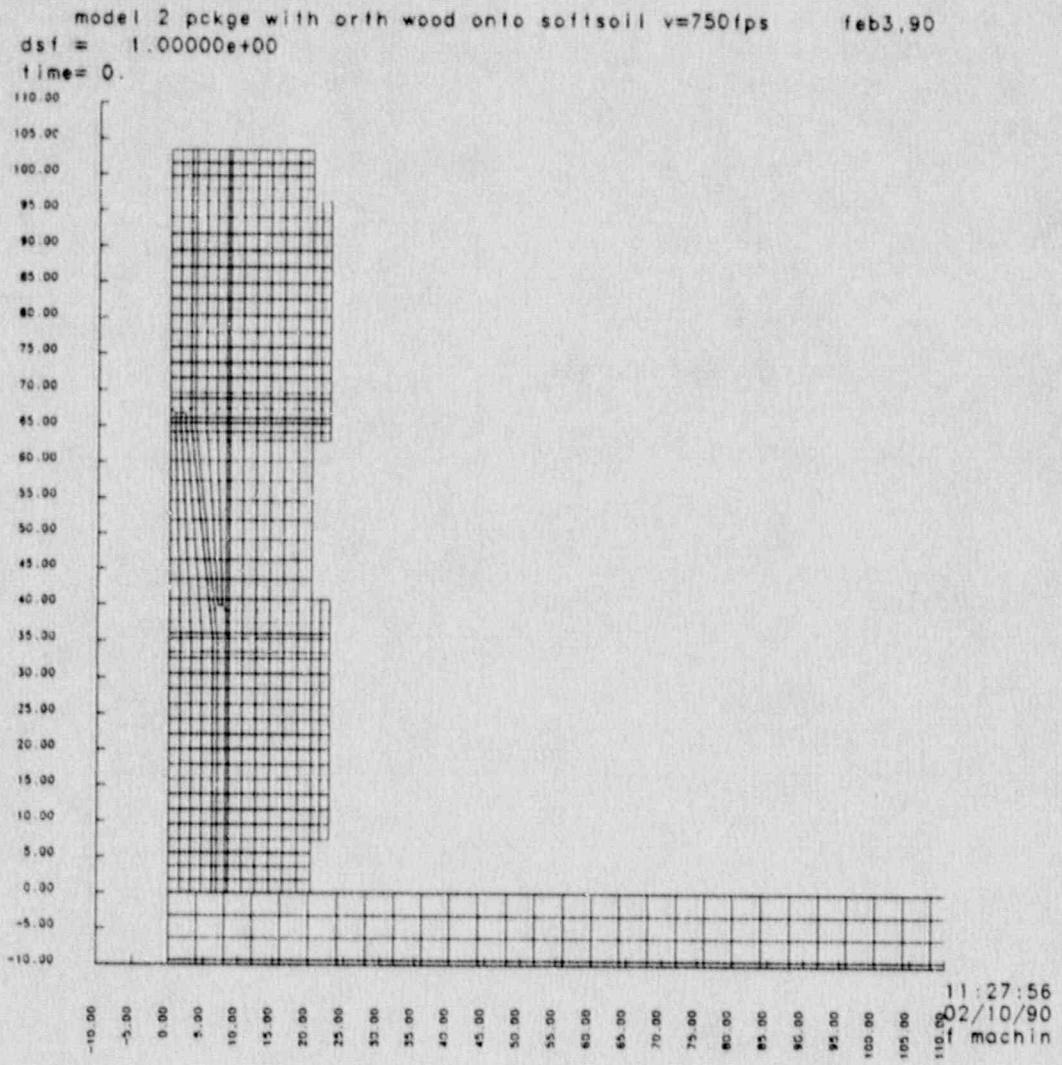

Fig. 4-2. Two-dimensional finite element mesh for end impact onto various surfaces.

4.2 Material Properties

Material properties for the package are as described in Section 2 of this report. Properties for the three target materials are discussed in Ref. 15, and are listed in Table 4-1. The weathered rock model is the "best estimate" of the PSA Flight 1771 crash site soil, and the granite and medium soil models are provided as "typical" of those two target types. The weathered rock model is a layered model, in order to match as closely as possible the layered conditions at the crash site.

Table 4-1. Soil and rock properties used with DYNA material Type 5 (See Ref. 15).

	Antelope Lake Soil[a] (Medium stiffness soil)	**Westerly Granite[b]**
Density, lb s^2/in^4	1.7523×10^{-4}	2.4635×10^{-4}
G, psi	5.0×10^4	1.43×10^6
K_u, psi	2.21×10^5	3.21×10^6
Yield curve constants:		
a^0	3.333×10^3	3.333×10^5
a^1	1.8×10	$9.805\ 10^3$
a^2	2.43×10^2	9.822×10^{-3}
Pressure cutoff, psi	-20.	-32.

Pressure/volumetric strain relationships

Pressure (psi)	$\ln\left(\frac{V_{new}}{V_o}\right)$	Pressure (psi)	$\ln\left(\frac{V_{new}}{V_o}\right)$
0.	0.	0.	0.
4.35×10	-1.258×10^{-2}	4.00×10^3	-1.83×10^{-3}
1.74×10^2	-2.532×10^{-2}	1.45×10^4	-5.961×10^{-3}
3.625×10^2	-3.563×10^{-2}	2.90×10^4	-1.0339×10^{-2}
1.305×10^3	-5.446×10^{-2}	4.35×10^4	-1.5665×10^{-2}
2.175×10^3	-5.922×10^{-2}	5.80×10^4	-2.0553×10^{-2}
5.8×10^3	-6.721×10^{-2}	7.25×10^4	-2.6637×10^{-2}
1.015×10^4	-7.796×10^{-2}	8.70×10^4	-3.1343×10^{-2}
2.9×10^4	-1.28×10^{-1}	1.015×10^5	-3.6783×10^{-2}

a Based on reports by Stephen Akers of WES, November 1986 and Woodward-Clyde Consultants, report to C. W. Young, March 1980.

b Based on a report by Heard, et al., 1974.

[NOTE: Input for soil and rock models is discussed in detail in Ref. 15.]

Table 4-1 - continued

PSA 1771 Weathered Rock

	Best Estimate Top Layer	Best Estimate Bottom Layer
Density, lb s^2/in^4	2.1950×10^{-4}	$2.1950\ 10^{-4}$
G, psi	1.264×10^5	1.264×10^5
K_u, psi	$5..90 \times 10^5$	4.57×10^5
Yield curve constants:		
a_0	2.2218×10^5	1.8×10^5
a_1	1.048×10^3	7.953×10^2
a_2	5.024×10^{-3}	$3.413\ 10^{-3}$
Pressure Cutoff, psi	-1.0×10^{-5}	-1.0×10^{-5}

Pressure/volumetric strain relationships

Pressure (psi)	$\ln\left(\frac{V_{new}}{V_o}\right)$	Pressure (psi)	$\ln\left(\frac{V_{new}}{V_o}\right)$
0.	0.	0.	0.
1.160×10^3	-1.283×10^{-2}	1.160×10^3	-9.000×10^{-3}
7.250×10^3	-3.542×10^{-2}	7.250×10^3	-5.520×10^{-2}
1.015×10^4	-4.416×10^{-2}	1.015×10^4	-7.260×10^{-2}
1.450×10^4	-5.758×10^{-2}	1.450×10^4	-9.250×10^{-2}
2.175×10^4	-7.553×10^{-2}	2.175×10^4	-1.129×10^{-1}
2.900×10^4	-9.365×10^{-2}	2.900×10^4	-1.397×10^{-1}
3.625×10^4	-1.079×10^{-1}	3.625×10^4	-1.687×10^{-1}
5.800×10^4	-1.480×10^{-1}	5.800×10^4	-2.141×10^{-1}

4.3 Analyses

End and side impact analyses were made for a range of velocities. Resulting decelerations are provided in Tables 4-2 through 4-4, and are plotted in Figs. 4-3 through 4-7.

Table 4-2. Two-dimensional finite element analyses for impact onto medium stiffness soil.

Velocity ft/s	Side		End	
	Δv/Δt (g)	Peak load (g)	Δv/Δt (g)	Peak load (g)
422	4130	4548	1967	2307
582	5760	6554	2166	2356
650	6563	7154	2210	2371
750	8002	8438	2345	2392

Table 4-3. Two-dimensional finite element analyses for impact onto PSA Flight 1771 weathered rock.

Velocity ft/s	2D Side		End	
	Δv/Δt (g)	Peak load (g)	Δv/Δt (g)	Peak load (g)
422	N/A	N/A	2842	3704
675	N/A	N/A	4022	5348
930	8484	10492	5665	6902

Table 4-4. Two-dimensional finite element analyses for impact onto granite.

Velocity ft/s	2D Side		End	
	Δv/Δt (g)	Peak load (g)	Δv/Δt (g)	Peak load (g)
422	6296	6391	3430	3787
582	6869	7636	5510	6464
650	7837	9538	5541	6953
750	8108	9411	11978	12089

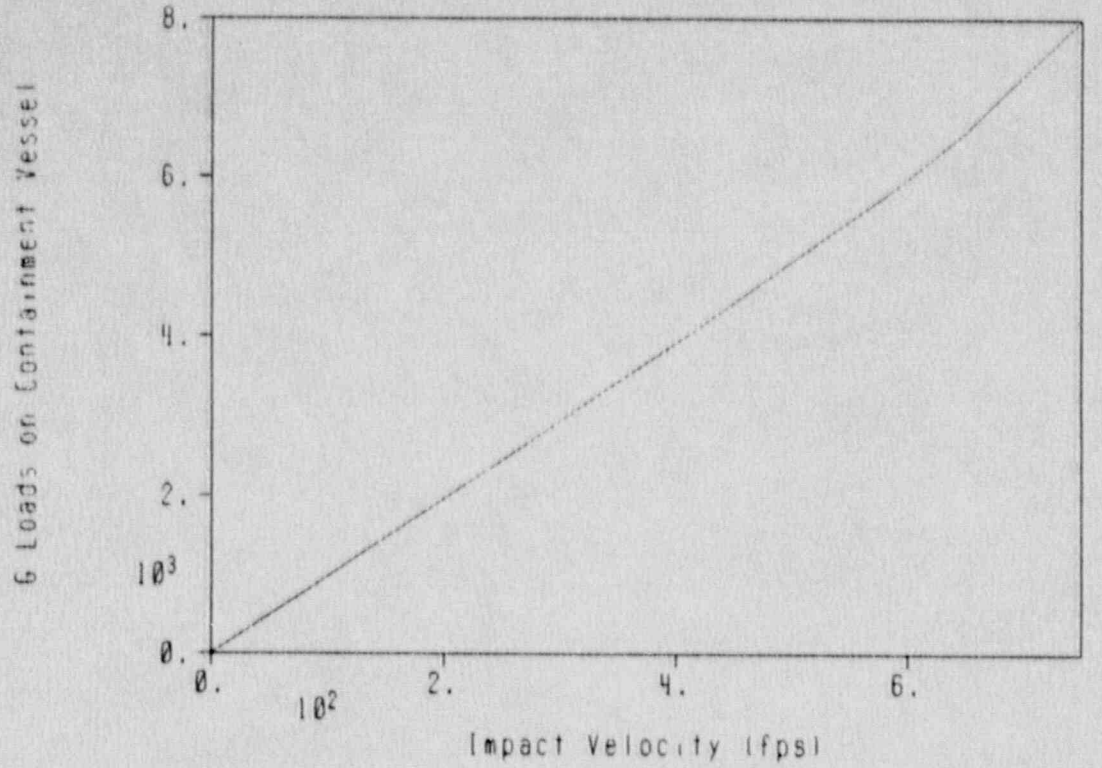

Fig. 4-3. Two-dimensional end impact onto medium stiffness soil.

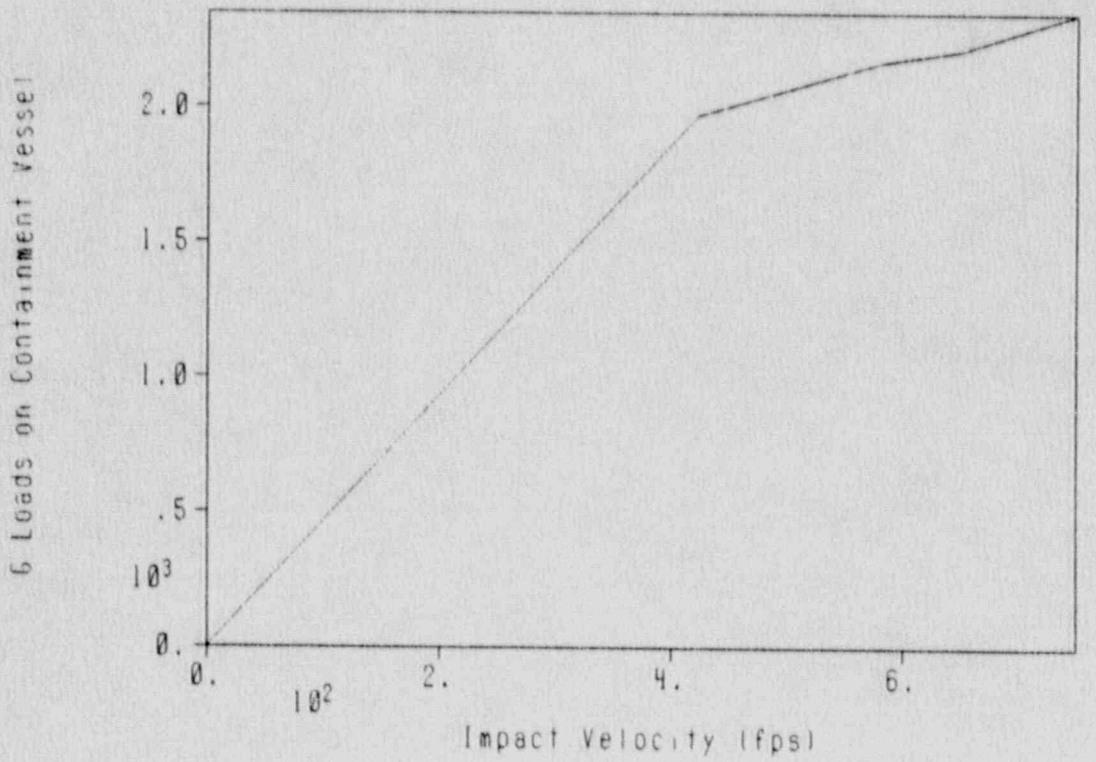

Fig. 4-4. Two-dimensional side impact onto medium stiffness soil.

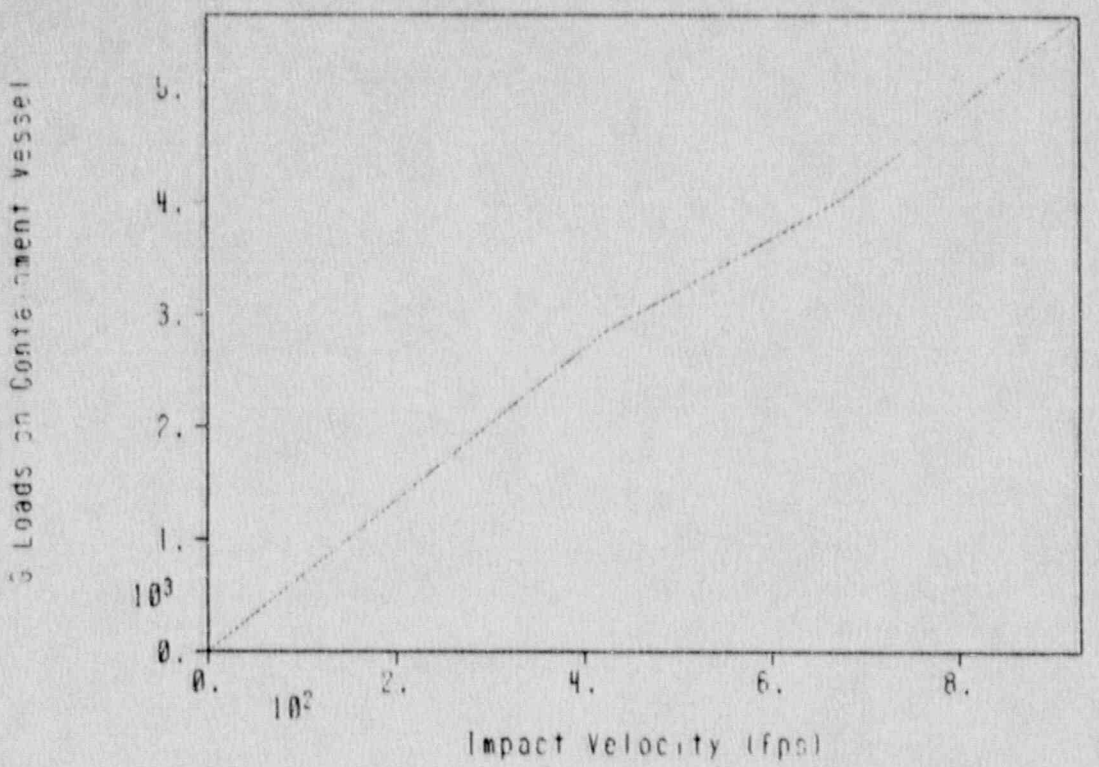

Fig. 4-5. Two-dimensional end impact onto PSA Flight 1771 weathered rock.

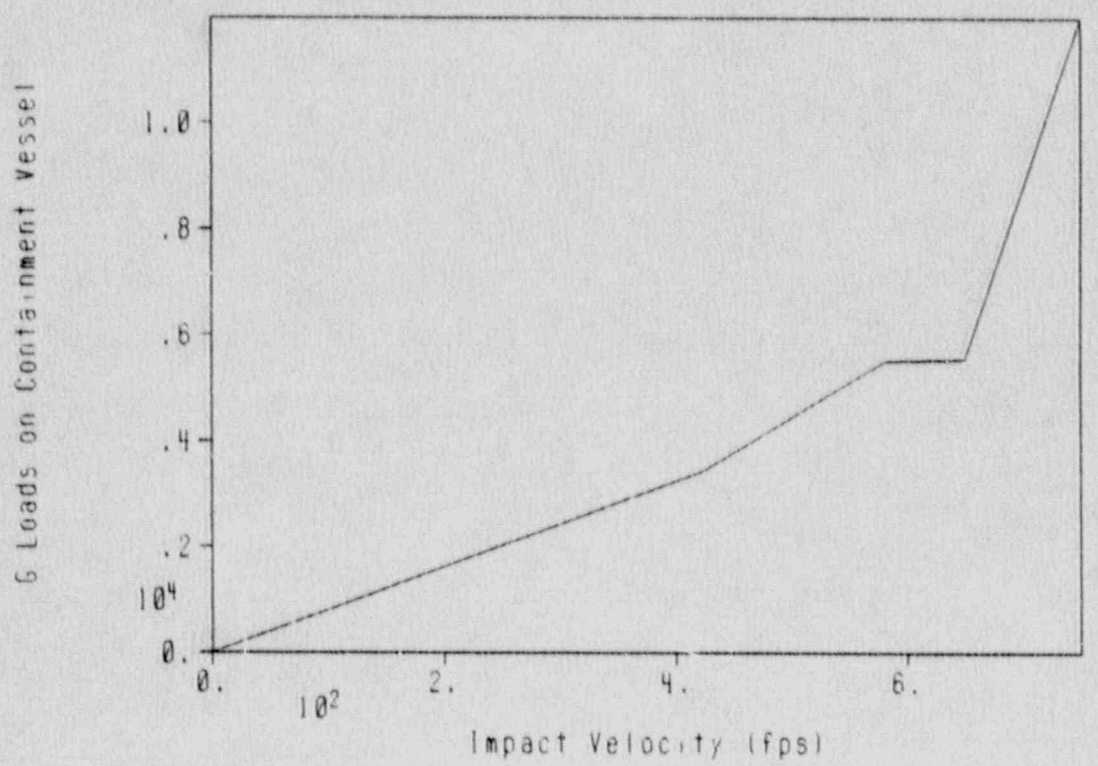

Fig. 4-6. Two-dimensional end impact onto granite.

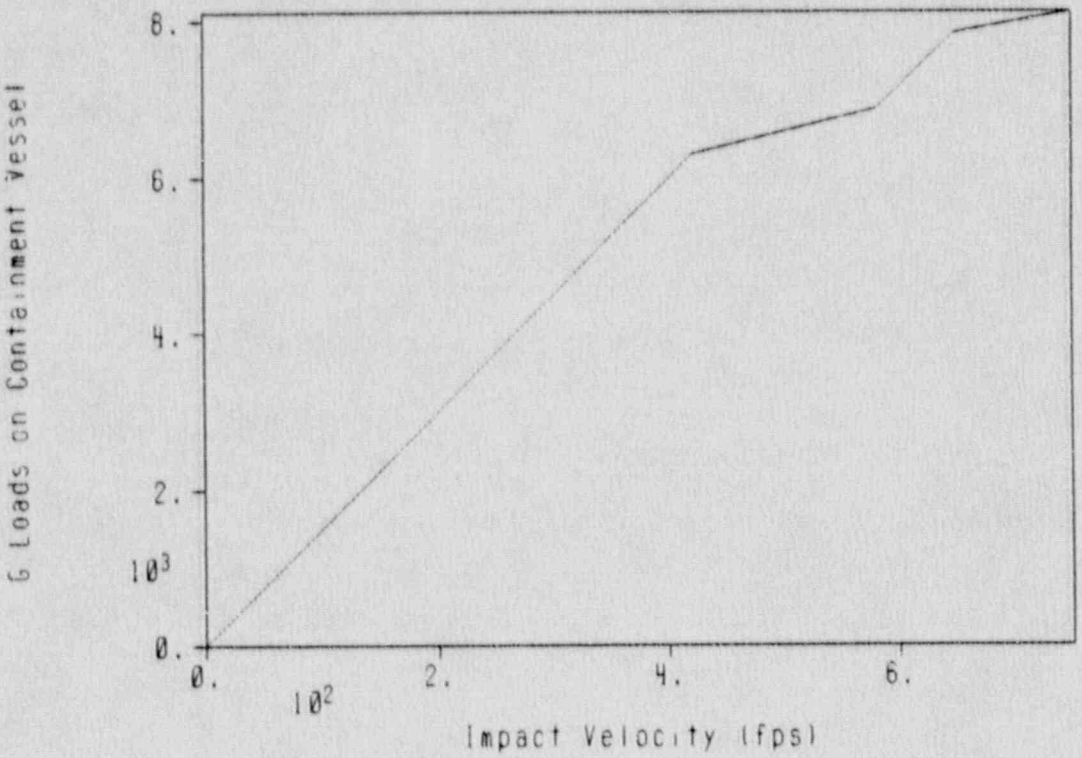

Fig. 4-7. Two-dimensional side impact onto granite.

4.4 Assumptions

Assumptions for these analyses are the same as those listed for impacts onto an unyielding surface in Section 3.4.

4.5 Conclusions

It is possible with the results provided in Sections 3 and 4, to estimate an "equivalent velocity" for impact onto an unyielding surface that produces the same average load on the outer containment vessel as for impact on the three impact materials considered. This is illustrated in Figs. 4-8 and 4-9.

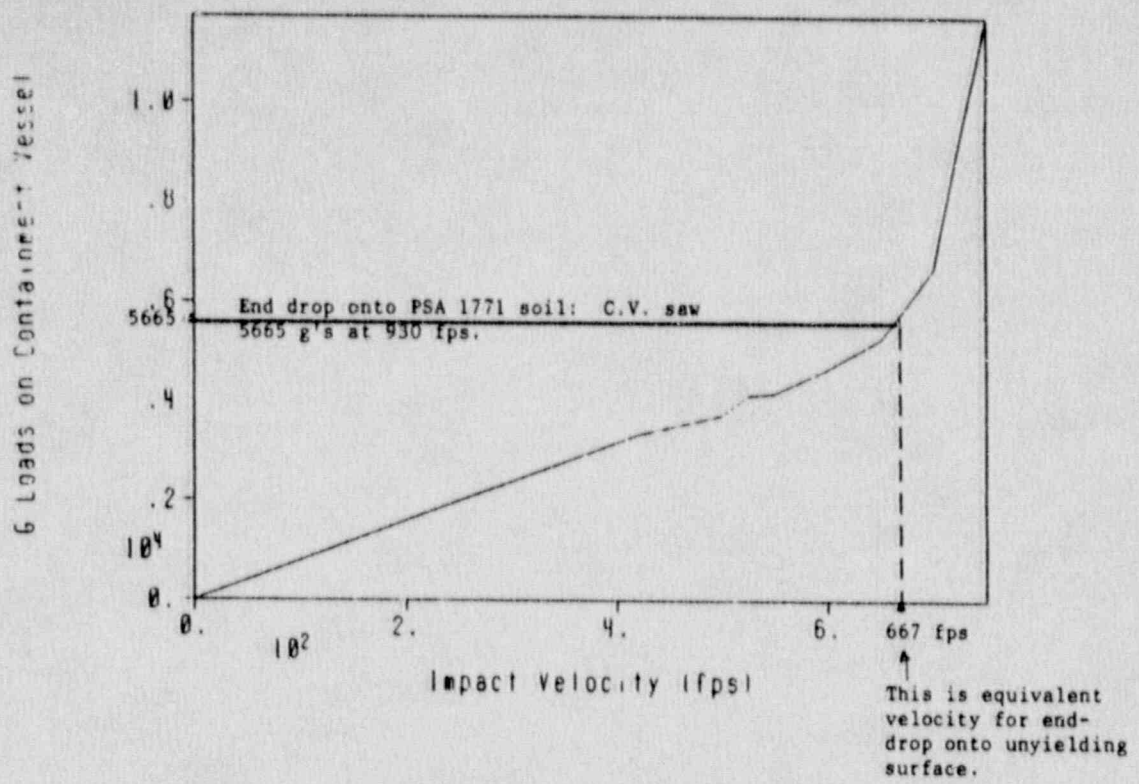

Fig. 4-8. Two-dimensional side impact (onto unyielding surface).

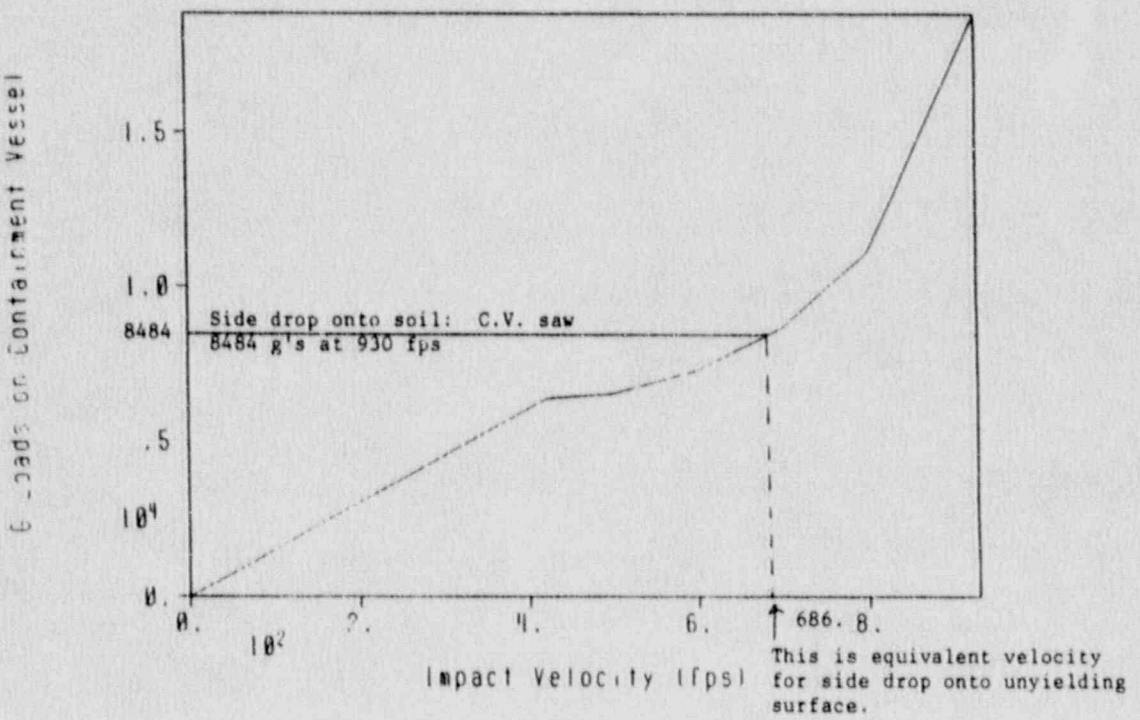

Fig. 4-9. Two-dimensional end impact onto unyielding surface.

5. PACKAGE-TO-PACKAGE INTERACTION DURING CRASH

A question which must be addressed with regard to the selection of aircraft which will be used during the crash test is: what is the effect of the number of packages which can be carried in the test and cargo aircraft? This question has been addressed in the following manner: an assumption is made that axisymmetric conditions exist in the fuselage at the time of impact. This assumption is incorrect to the extent that the aircraft crash test criteria do not require impact perpendicular to the ground surface, but at an angle of >60°. However, since judgment indicates that direct end-to-end contact would produce the worst impact conditions in the package, (not including possible puncture due to impact with aircraft components), the analyses for package-to-package interaction were performed using axisymmetric models. A simplified package model was used for these analyses, as shown in Fig. 5-1. The following assumptions were made: first, there is no transverse interaction between the packages (corresponding to the axisymmetric assumption); second, there are five packages in a single, lengthwise row in the fuselage; and third, the packages do not interact with the fuselage (i.e., they fall directly onto the rock material).

The finite element model used for the analyses is shown in Fig. 5-2. Analyses were made with two targets: hard rock and weathered rock. Properties assumed for these materials are listed in Table 5-1. The packages are spaced 40 inches apart in the analyses. In order to decrease the computation time required to perform the multiple package impacts, a technique was used which eliminated the soil from the analyses after the first package came to rest. The procedure is as follows: run the complete mesh (seen in Fig. 5-2) enough time steps so that the first package comes to a complete stop (at this point the second package also comes to nearly a complete stop). Determine the velocity time history for one node at the base of the package (see Fig. 5-3). Generate an identical finite element mesh, but eliminate the target material. Apply the velocity time history from Fig. 5-3 to all of the nodes at the base of the first package, while at the same time applying the impact velocity to each of the five packages. Velocity and acceleration results using this method can be seen in Figs. 5-4 and 5-5. These results can be compared with the velocity and acceleration results for the mesh with the soil on Figs. 5-6 and 5-7. It can be seen that the shapes and peak values in the plots are very similar. Results are listed in Table 5-2.

The overall conclusion to be reached from these analyses is that the first package sees the highest load due to impact, regardless of how many other packages are in line behind it, for impacts onto the two types of rock considered. This is not surprising in light of the fact that all impacts after the first have twice as much impact limiting material as the first.

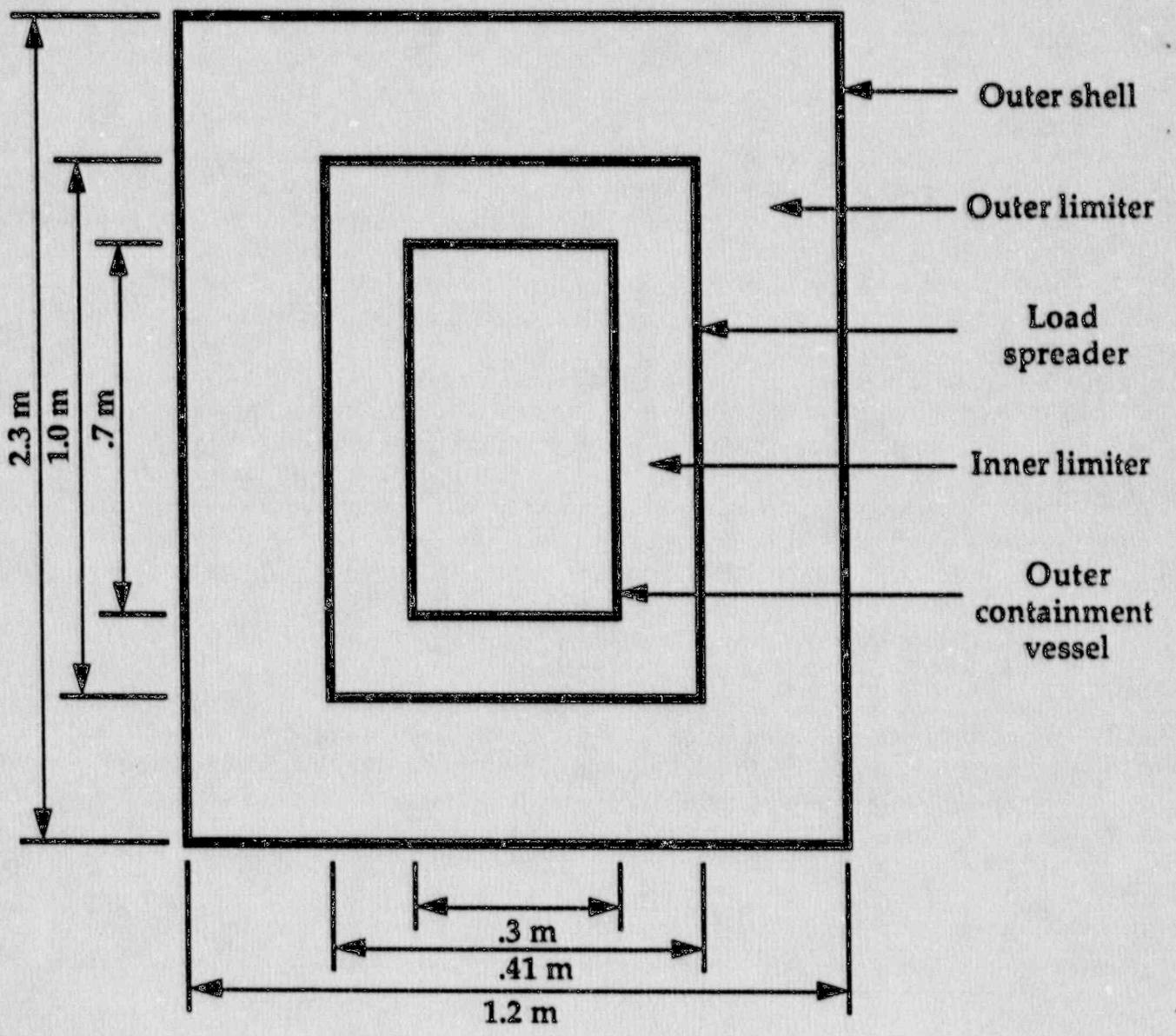

Fig. 5-1. Basis package model used for package-to-package analysis.

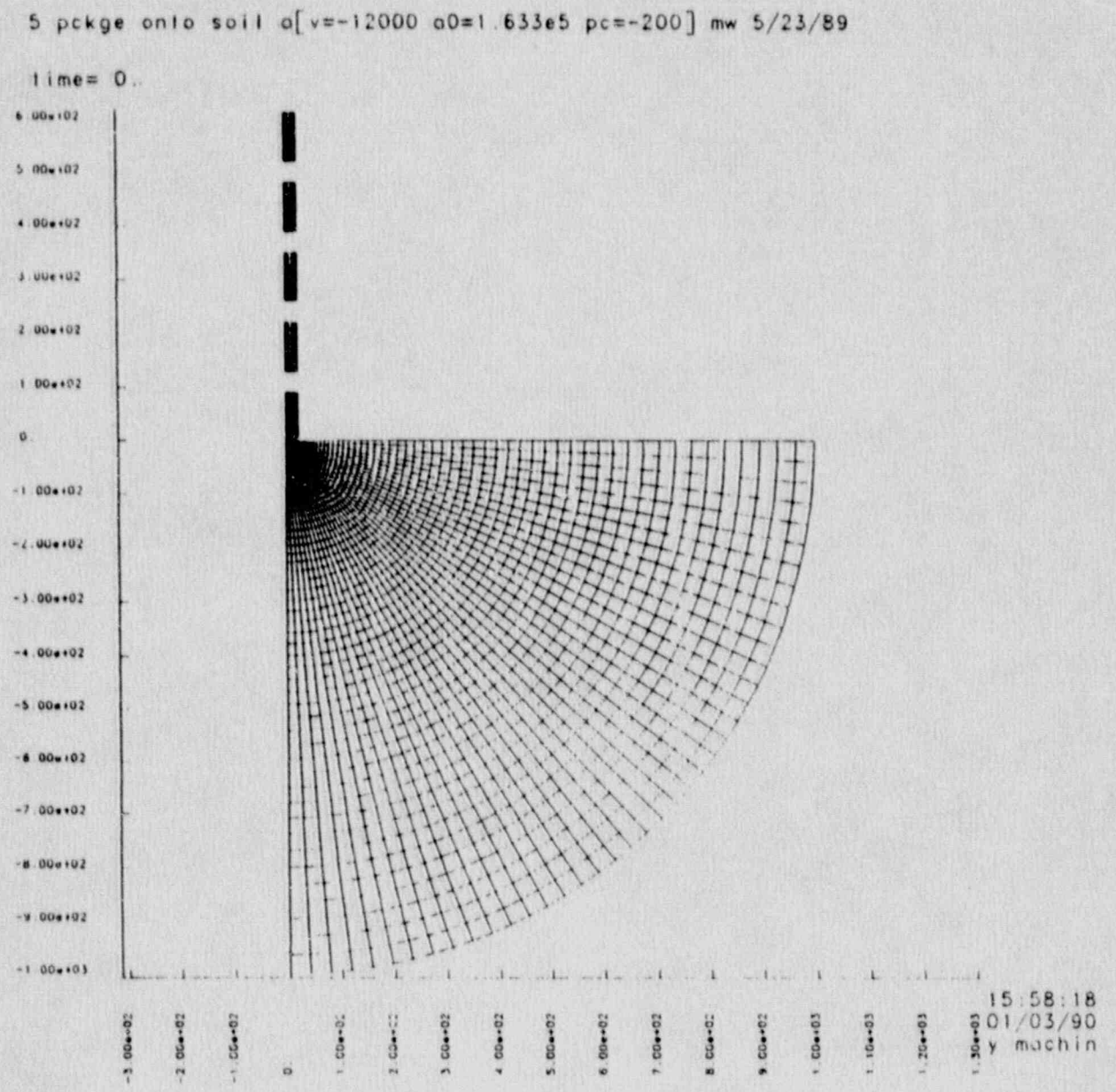

Fig. 5-2. Finite element mesh used for package to package interaction analyses.

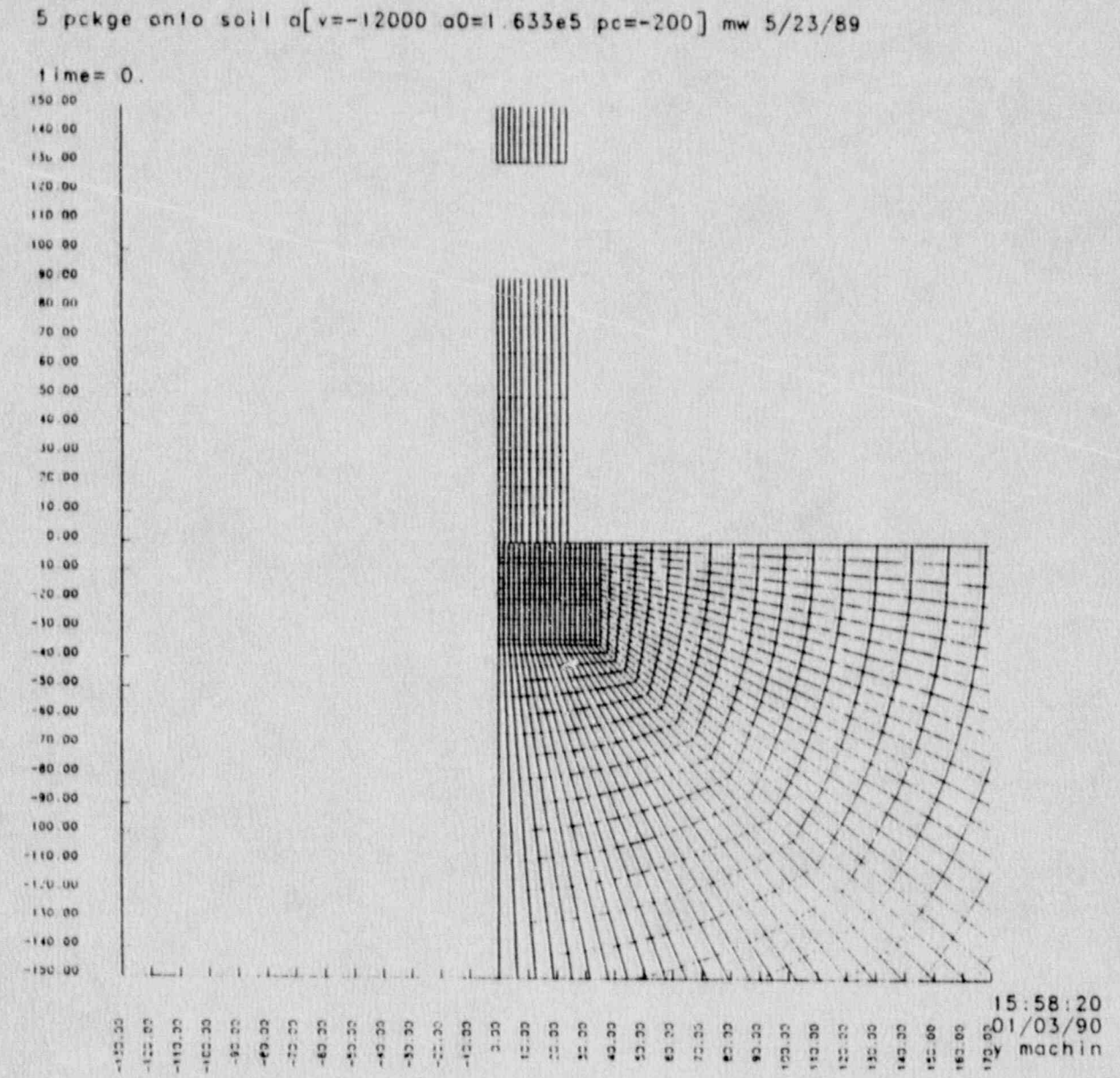

Fig. 5-2-continued

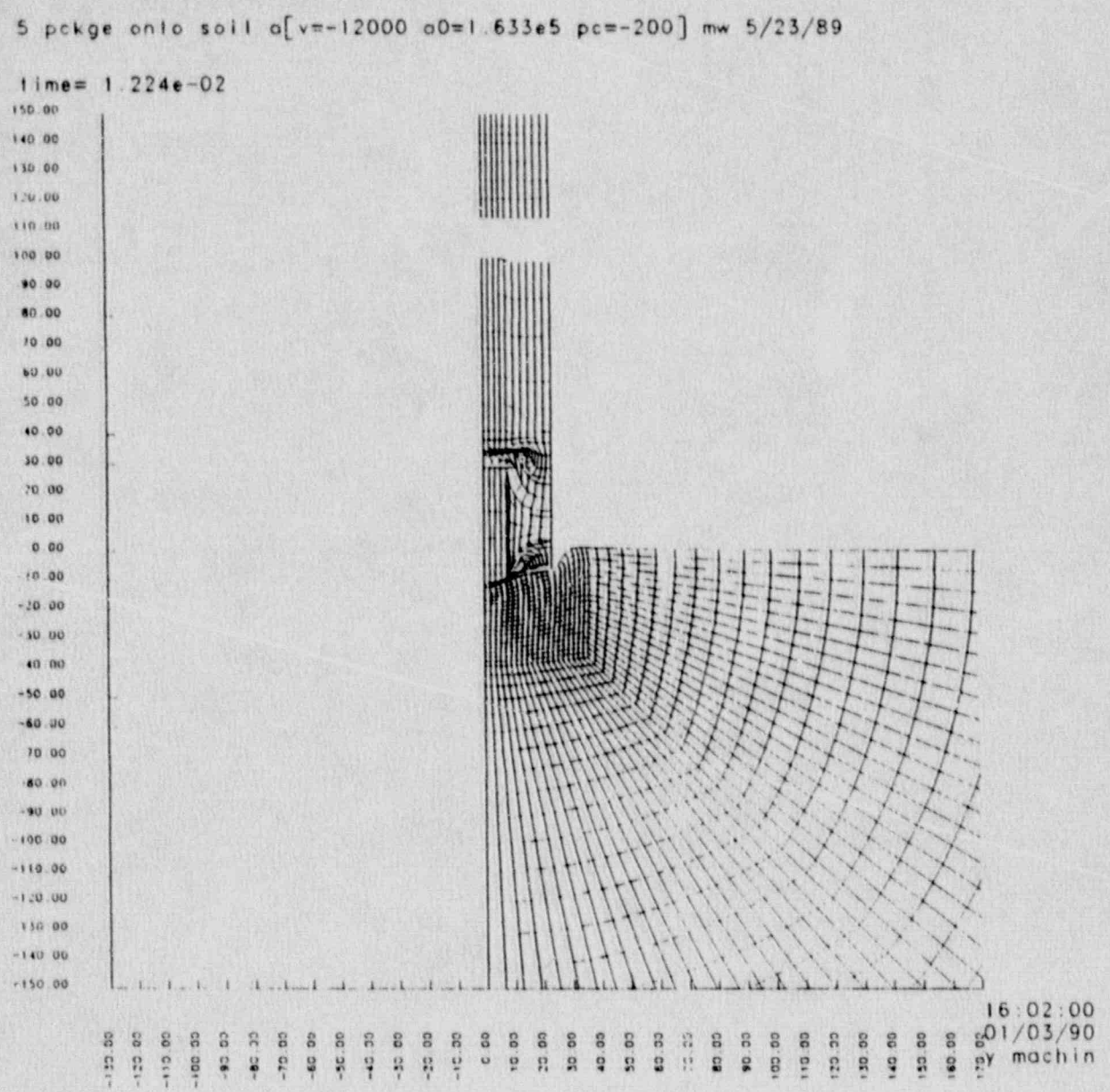

Fig. 5-2- continued

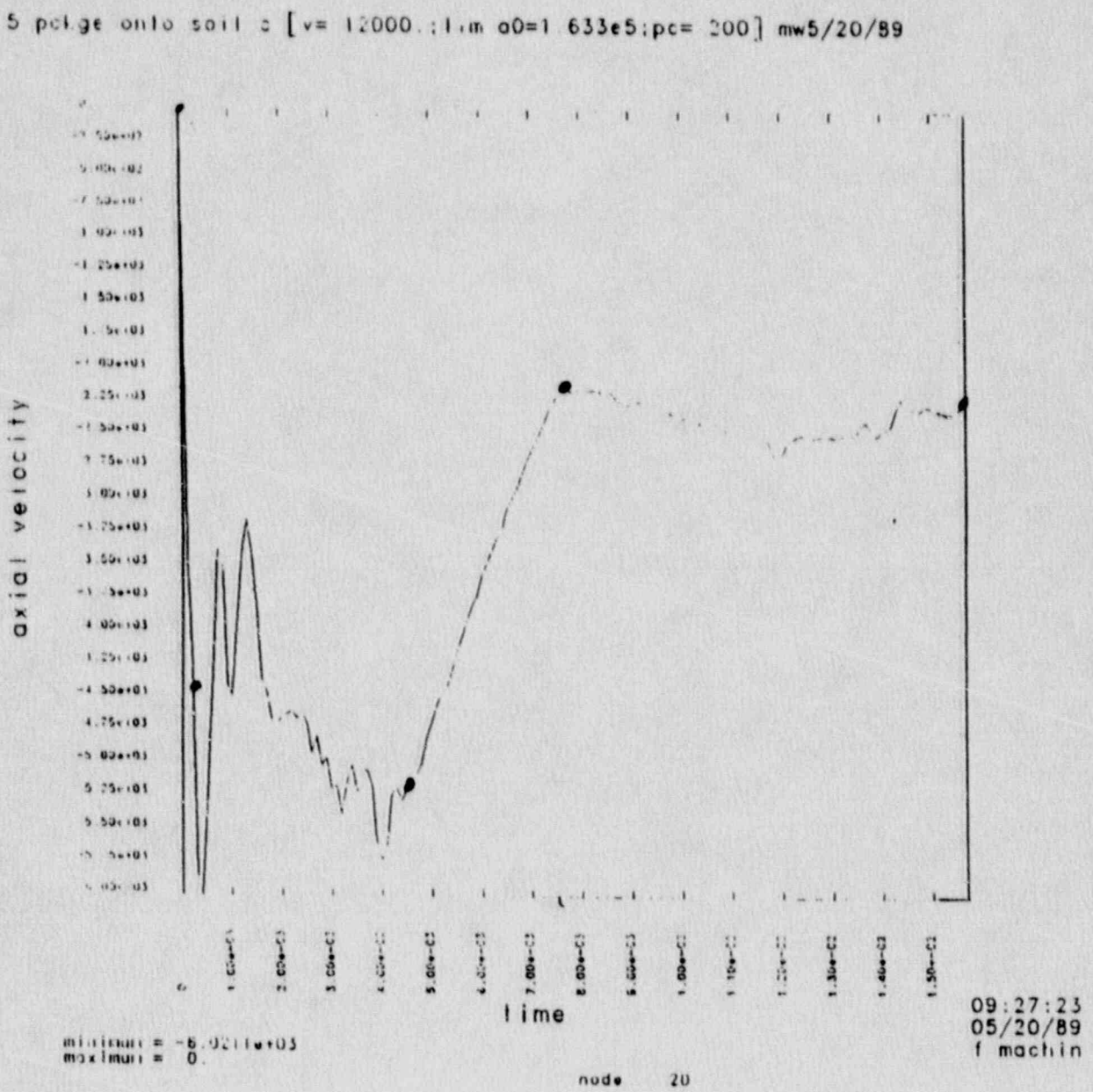

Fig. 5-3 Velocity time history of a node at the bottom of the impact limit on the first package during impact at 1000 ft/s.

Table 5-1. Properties for soils used in package-package analyses.

	Hard Rock	Weathered Rock
Density, lb s^2/in^4	1.56×10^{-4}	1.47×10^{-4}
Shear modulus, psi	3.5×10^{5}	6.00×10^{4}
Bulk unloading modulus, psi	5.58×10^{5}	1.06×10^{5}
Pressure cutoff, psi	-1.0×10^{-5}	-1.0×10^{5}
Yield curve constants:		
a_0	1.44×10^{5}	2.58×10^{5}
a_1	1.373×10^{3}	4.693×10^{2}
a_2	-1.40×10^{-5}	2.13×10^{-1}

Pressure/volumetric strain relationships

Pressure (psi)	$\ln\left(\frac{V_{new}}{V_o}\right)$	Pressure (psi)	$\ln\left(\frac{V_{new}}{V_o}\right)$
0	0	0	0
1.5×10^{5}	-3.6×10^{-1}	2.7×10^{4}	-3.6×10^{-1}
2.6×10^{5}	-6.9×10^{-1}	4.5×10^{4}	-6.9×10^{-1}
4.0×10^{5}	-1.4	6.8×10^{4}	-1.4

*Note: V is the relative volume of the material, defined as $V = \ln\left(\frac{V_{new}}{V_{original}}\right)$.

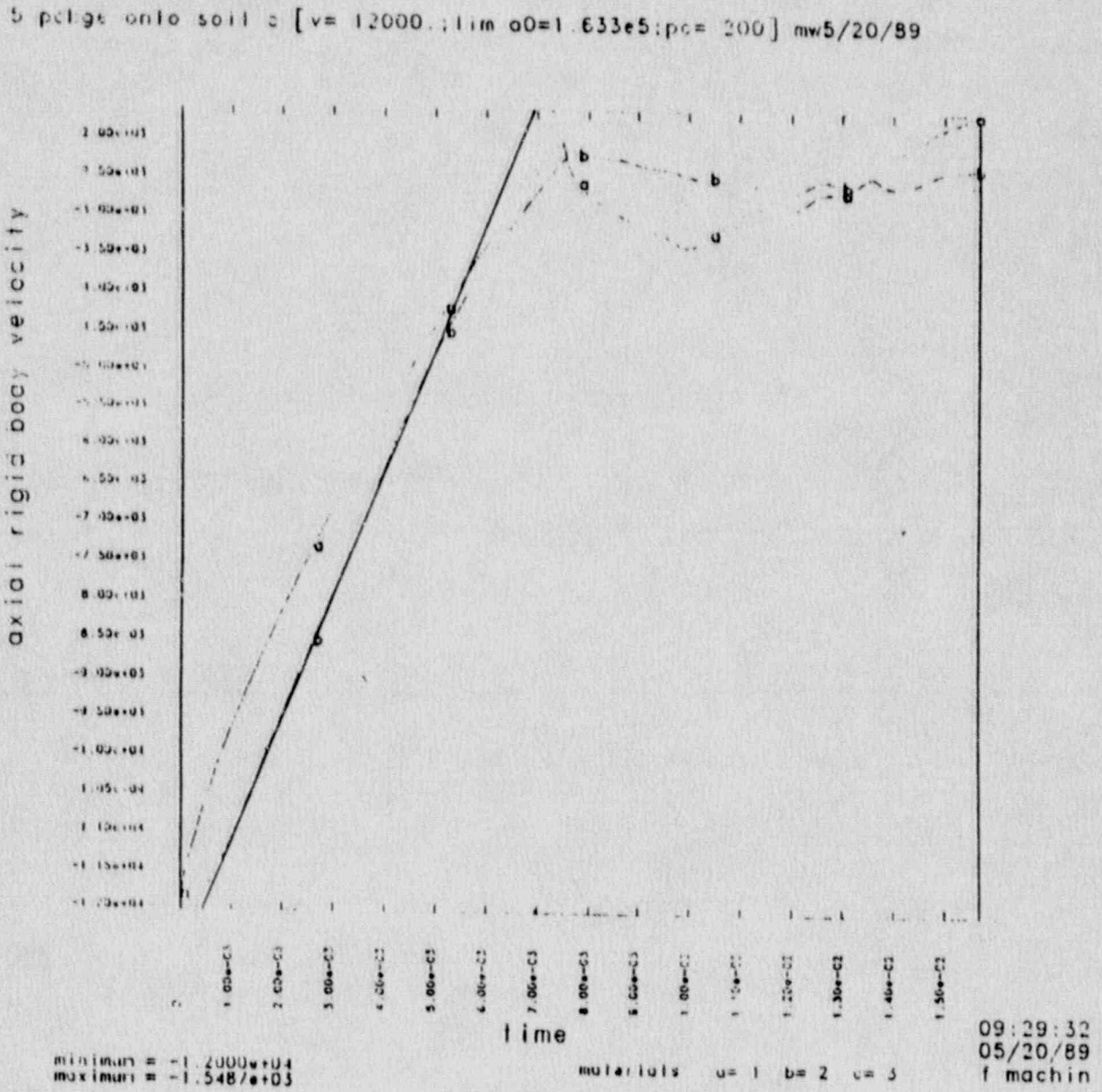

Fig. 5-4. Velocity-time history of the outer containment vessel of the lowest package.

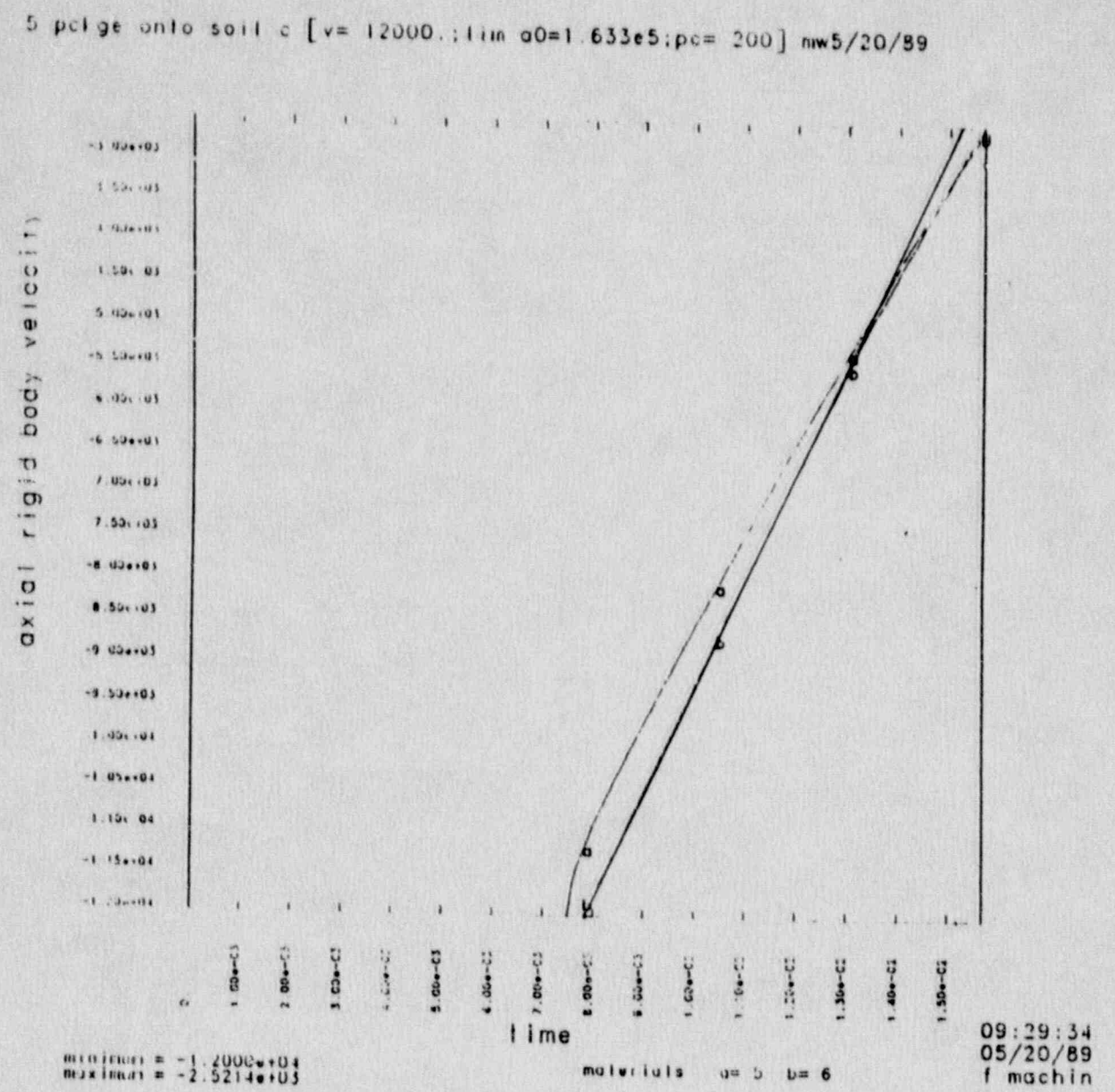

Velocity - Time history of the outer containment vessel of the next to the lowest package during impact.

Fig. 5-4-continued

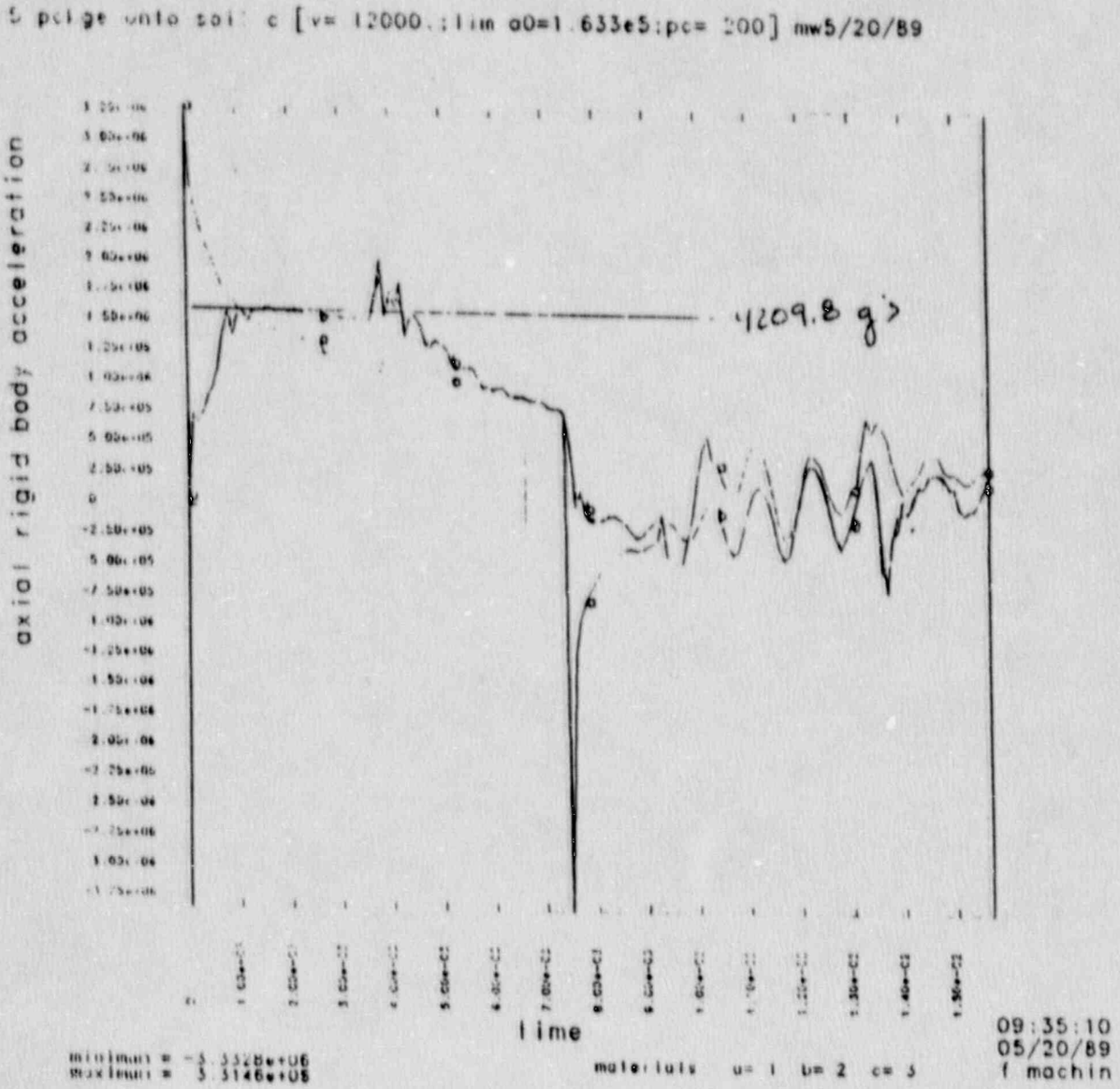

Fig. 5-5a. Acceleration time history of the outer containment vessel of the lowest package during impact.

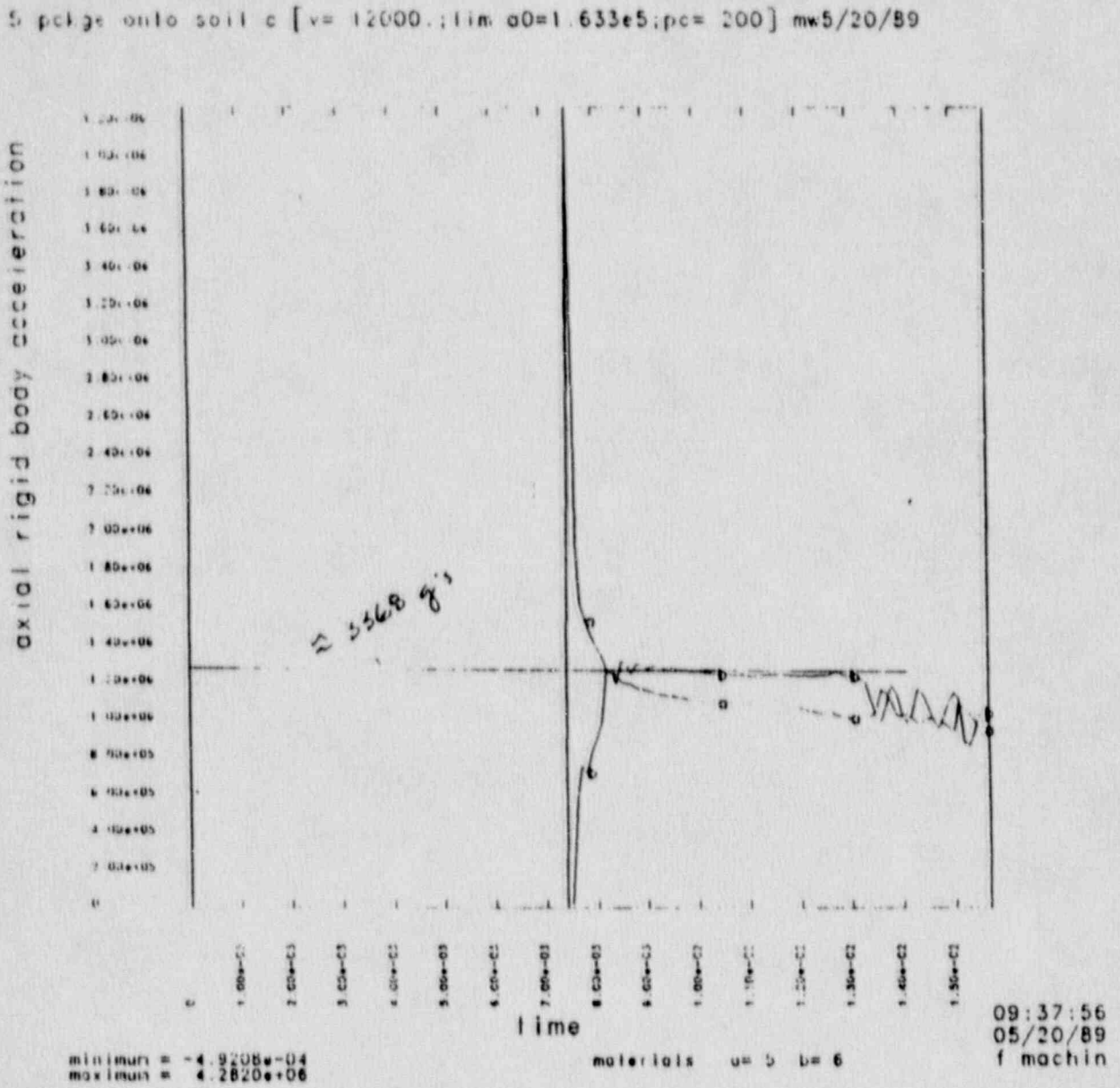

Fig. 5-5b. Acceleration time history of the outer containment vessel of the second package during impact.

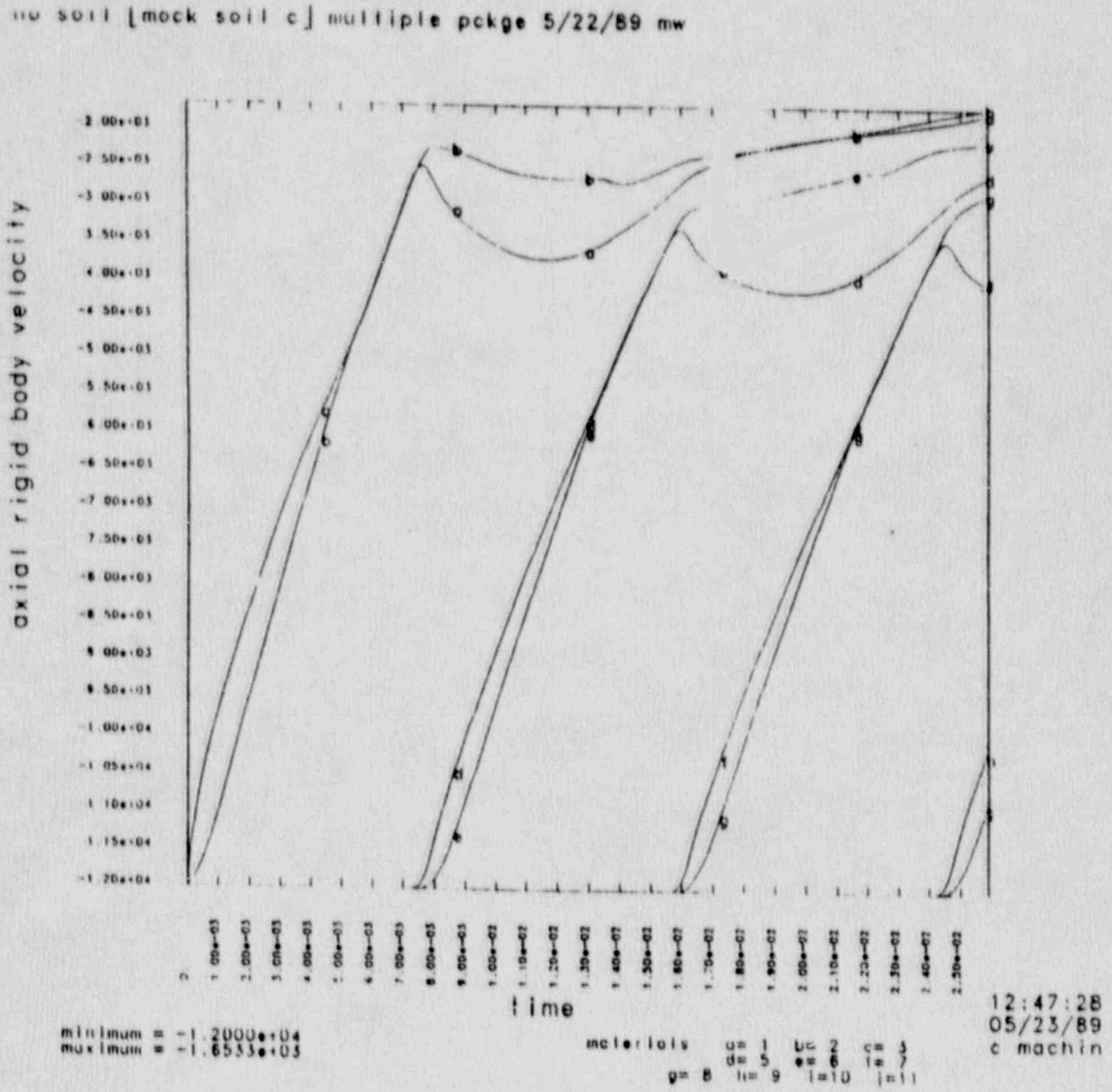

Fig. 5-6. Velocity time histories of the first through fourth packages during impact using the modified mesh.

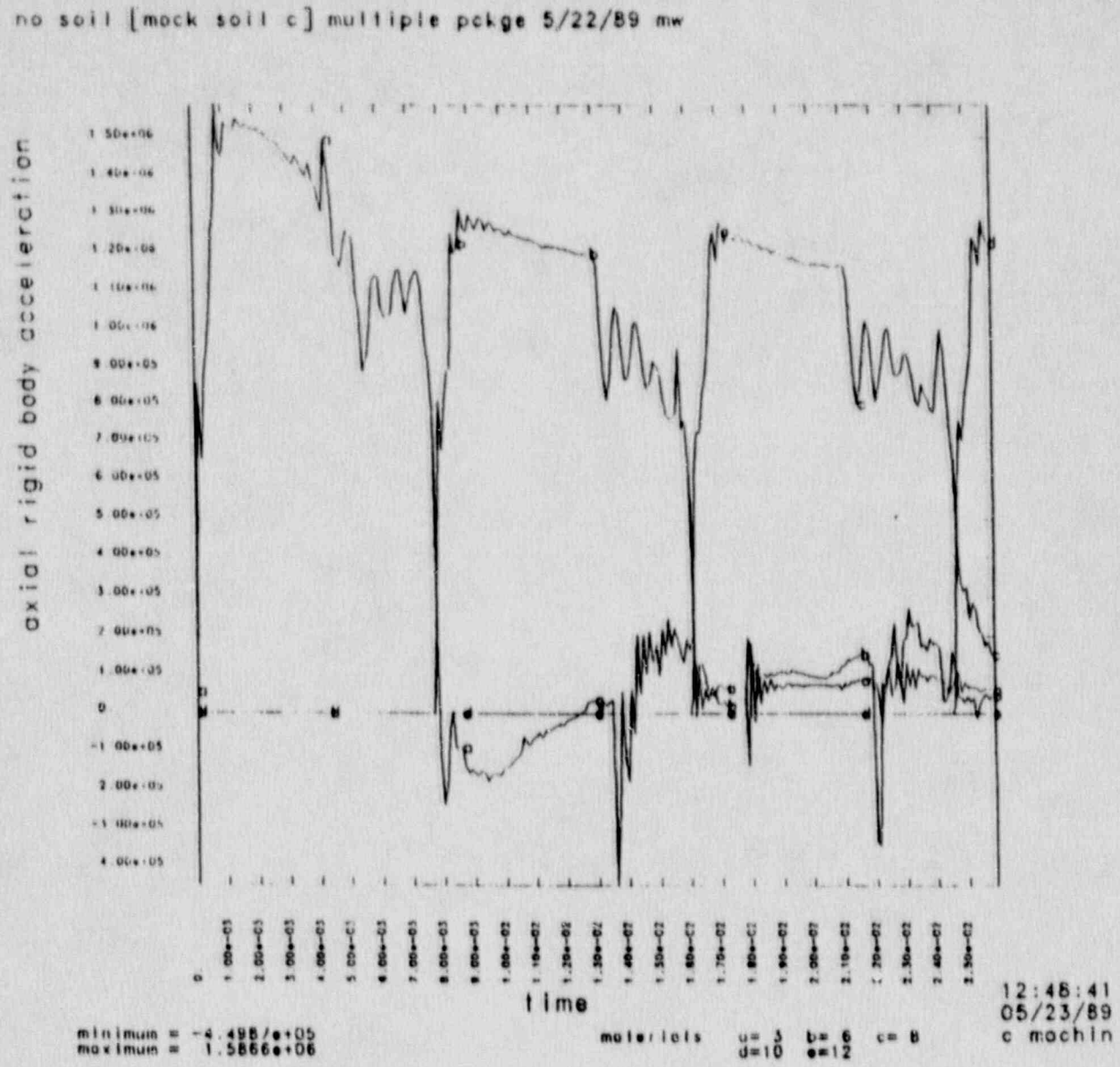

Fig. 5-7. Acceleration-time histories of the first through fourth package during impact, using the "no soil" model.

Table 5-2. Summary of loads acting on the inner container.

Package	Average load, g	
	Hard Rock	Weathered Rock
1 (first to impact)	12700	4200
2	8700	3350
3	N/A*	3200
4	N/A*	3200
5	N/A*	N/A*

* N/A = not available

6. SIMPLIFIED ANALYSES OF FUSELAGE IMPACTS ONTO SOIL

In order to evaluate the contribution of the aircraft to the loads which the package will experience during a nose-down aircraft impact, several issues must be addressed. One is the effect of the number of packages which may be carried in a single aircraft transport. This problem is addressed in Section 5 of this report. Another issue is the effect of the aircraft components themselves if they impact the package. This problem will be addressed separately. The third issue concerns the hardness of the ground at the time the package strikes the ground and whether a larger or heavier aircraft will compact the ground more than a smaller or lighter one.

6.1 Geometry and Mesh

In order to evaluate the impact of the fuselage on the soil, several finite element models were tried. The first was a 3D shell model section, with density increased so that the weight of the shell included the weight of the fuselage plus contents. At the high impact velocity desired this model buckled and "crashed" long before 10% of the aircraft kinetic energy was dissipated. The next model attempted was a "solid" fuselage 2D axisymmetric model, using a crushable material model, with aluminum properties scaled down to take into account the larger cross sectional area. This model was cylindrical, with roughly conical nose and tail sections. It also included the weight of the fuselage plus contents. This model performed better, but was still unable to effectively dissipate the kinetic energy before becoming unrealistic. The third and final model attempted was a simple solid cylinder, with outside diameters and length equal to the average fuselage outside diameter and full length of the aircraft. A crushable material model was used to represent the aircraft as it impacted a semi-infinite half-space target model, with a slideline between the fuselage and the soil target. This model performed well, however, it represents a substantial simplification of the actual fuselage impact geometry. The mesh is shown in Fig. 6.1.

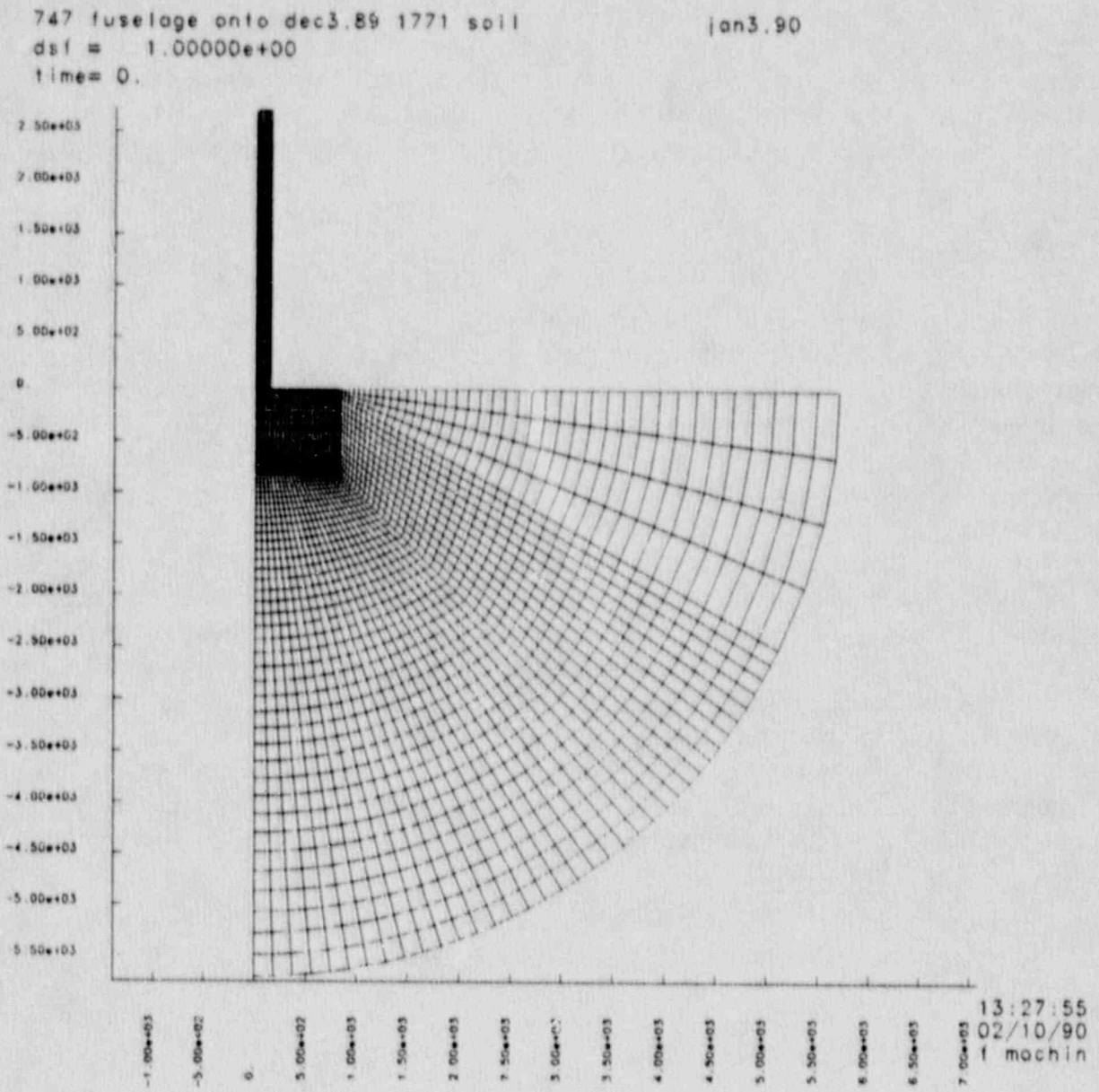
747 fuselage onto dec3.89 1771 soil
jan3.90
dsf = 1.00000e+00
time= 0.
13:27:55
02/10/90
f machin

Fig. 6-1

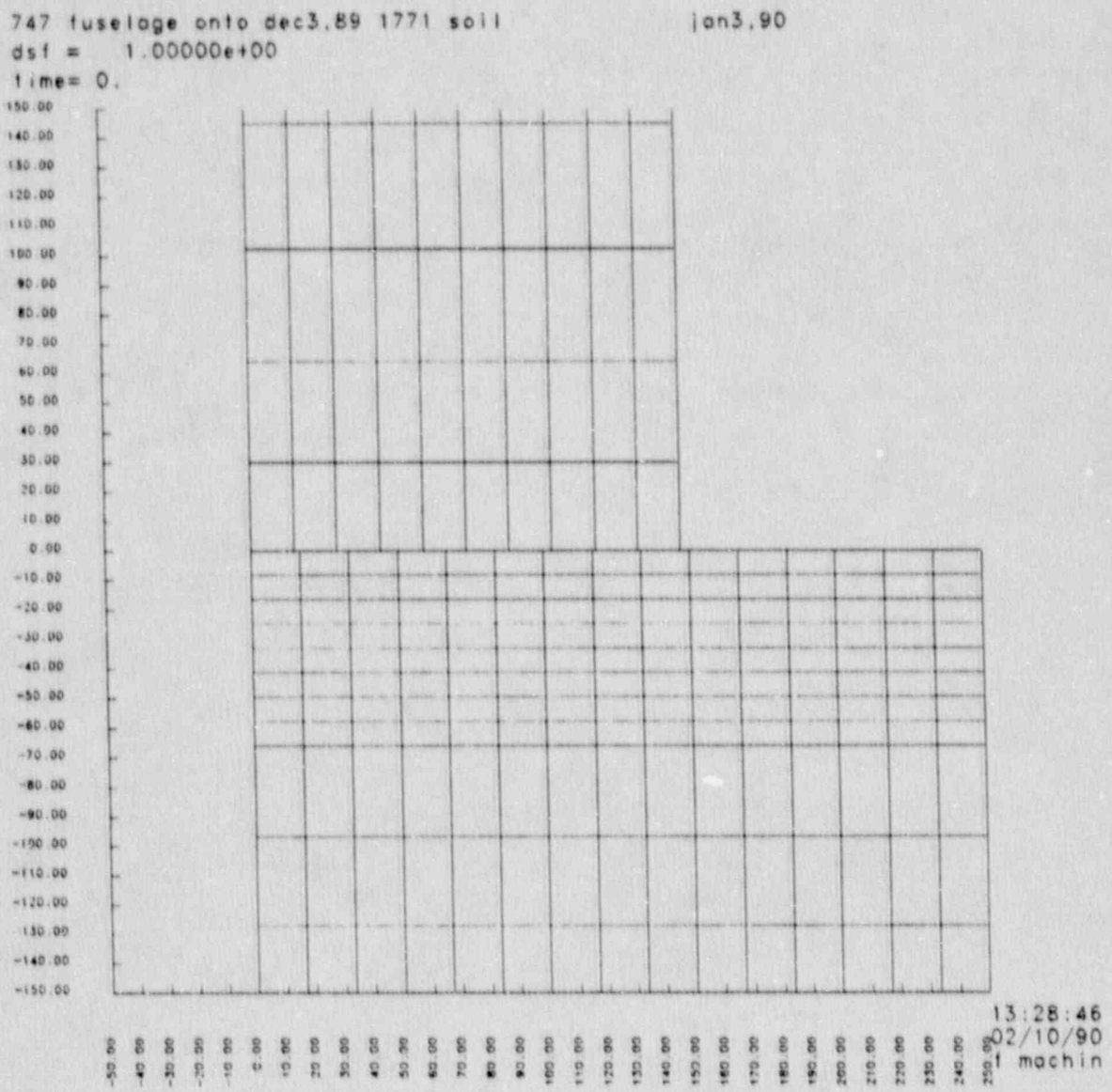

Fig. 6-1 - continued

6.2 Materials

The two-layer soil target is representative of PSA Flight 1771 impact material. The material model development is documented in Ref. 15. The soil is modeled with DYNA's material Type 5. Material properties are provided in Section 4, Table 4-1.

The fuselage is also modeled with DYNA's material Type 5. The property development is illustrated below for a B-747 aircraft based on the following information:

	B-747	B-707
Aircraft weight, empty, zero-fuel, lb	327,000	146,400
Fuselage radius, in	147	76
Fuselage length, in	2702	1740

Volume of the B-747 (as modeled) = π x radius^2 length

= $(\pi)\ (147)^2\ (2702) = 1.83 \times 10^8$ in^3.

$$\text{Approx. volume of actual aircraft} = \frac{\text{weight of aircraft (net)}}{\text{density of aluminum}}$$

$$= \frac{327000 \text{ lb}}{0.1 \text{ lb/in}^3} = 3.27 \times 10^6 \text{ in}^3$$

$$\sigma \text{ yield, model} = \frac{\text{Vol.}_{\text{actual}}}{\text{Vol.}_{\text{model}}} \cdot \sigma \text{ yield, actual}$$

$$= \frac{3.27 \times 10^6}{1.83 \times 10^8} \times (40{,}000)$$

$$= 713.2 \text{ psi}$$

$$\text{density, model} = \frac{\text{aircraft weight}}{\text{Vol. model}}$$

$$= \frac{737\,500 \text{ lb}}{1.834 \times 10^8 \text{ in}^3} = 4.02 \times 10^{-3} \text{ lb/in}^3$$

Material properties as input for the B-747 and B-707 "solid" fuselage models are provided in Table 6-1.

Table 6-1. Properties used for the fuselage impact analyses.

	B-747	B-707
Density, lb s^2/in^4	1.042×10^{-5}	1.473×10^{-5}
G, psi	1.0×10^5	1.0×10^5
K_u, psi	1.2×10^6	1.2×10^6
Yield curve constants:		
a_o	1.695×10^5	3.39×10^5
a_1	0	0
a_2	0	0
Volumetric strain/pressure relationship		
Vol. strain: $\ln\left(\frac{V_{new}}{V_o}\right)$	Pressure (psi)	
0.	0.	0.
-.001	713.	1008.
-1.2	713.	1008.
-2.3	1.1×10^6	1.1×10^6

6.3 Results and Conclusions

The fuselage impacts were run at 930 ft/s. Results are provided in Table 6-2. The results of these simple analyses indicated that there is not a substantial difference between the B-707 and B-747 fuselage impacts. The B-707 impact shows slightly more soil compaction, slightly higher soils pressure, larger crater depth, and roughly equivalent accelerations. If anything, the results indicate that using a B-707 in the test crash would be a conservative test for the B-747 impact, without consideration of crush and puncture loads.

Table 6-2. Results from analyses of fuselage impacts onto PSA Flight 1771 ground material.

	Aircraft Type	
	B-707	B-747
Kinetic energy remaining at conclusion of analyses, %	0.8	0.1
Average of peak loads in fuselage, g	689	516
Peak load in nodes 1 & 10 (on lower surface of fuselage), g	54231	59474
Peak load in nodes 1 & 10 after initial spike, g	9844	3886
Max. volumetric strain in compression	-.0491	-.0317
Max. pressure in PSA Flight 1771 ground material	12800 psi	6640 psi
Depth of "crater"	81.4"	38"
Depth of crater at t = 0.1 s.	81.4"	25"

7. REFERENCES

1. U.S. Nuclear Regulatory Commission, *Plutonium Air Transportable Package Model PAT-1: Safety Analysis Report*, NUREG-0361, 1978.

2. M. G. Stout and P. S. Follansbee, *Strain Rate Sensitivity, Strain Hardening, and Yield Behavior of 304L Stainless Steel*. Transactions of the ASME, Journal of Engineering Materials and Technology, Oct. 1986, Vol. 108, pgs. 344-353.

3. G. R. Johnson et al., *Response of Various Metals to Large Torsional Strains Over a Large Range of Strain Rates*, Part 2: Less Ductile Metals, Transactions of the ASME, Journal of Engineering Materials and Technology, Jan. 83, pgs. 48-53.

4. G. R. Johnson et al., *Response of Various Metal to Large Torsional Strains Over a Large Range of Strain Rates*, Part 1: Ductile Metals, Transactions of the ASME, Journal of Engineering Materials and Technology, Jan. 83, Vol. 105, pg. 42-47.

5. T. Nicholas and J. E. Lawson, *On the Determination of the Mechanical Properties of Materials at High Shear-Strain Rates*, J. Mech. Phys. Solids, 1972, Vol. 20, pgs. 57-64.

6. A. Gilat and R. J. Clifton, *Pressure-Shear Waves in 6061-T6 Aluminum and Alpha-Titanium*, J. Mech Phys. Solids, Vol. 33, No. 3, pgs. 263-284, 1985.

7. J. A. Liska, *Effect of Rapid Loading on the Compressive and Flexural Strength of Wood*, Report No. R1767, Forest Products Laboratory, Forest Service, U.S. Department of Agriculture, 1950.

8. M. P. Brokaw and G. W. Foster, *Effect of Rapid Loading and Duration of Stress on the Strength Properties of Wood Tested in Compression and Flexure*, Report No. 1518, Forest Products Laboratory, Forest Service, U.S. Department of Agriculture, 1952.

9. L. W. Wood, *Relation of Strength of Wood to Duration of Load*, Report No. 1916, Forest Products Laboratory, Forest Service, U.S. Department of Agriculture, 1951.

10. W. L. James, *Dynamic Strength and Elastic Properties of Wood*, Forest Products Journal, Vol. XII, No. 6, June 1962, pgs. 253-260.

11. H. Sugiyama, *On the Effect of the Loading Time on the Strength Properties of Wood*, Wood Science and Technology, Vol. 1, 1967, pgs. 289-303.

12. J. A. Anderson, *Plutonium Accident Resistant Container Project*, SAND78-0724, Sandia National Laboratories, May 1978.

13. T. Baumeister, et al., *Mark's Standard Handbook for Mechanical Engineers*, eighth ed., McGraw-Hill Book Company, New York, NY, 1978..

14. J. O. Hallquist, *User's Manual for DYNA2D—An Explicit Two-Dimensional Hydrodynamic Finite Element Code with Interactive Rezoning*, UCID-18756.

15. J. C. Chen and M. Witte, PATC-IR 89-12, *Development of Soil/Rock Constitutive Models and Benchmark Analysis for Gas-Gun Penetration Tests at the PSA Flight 1771 Crash Site*, publication forthcoming, March 22, 1990.